Facies and architecture of the SCIc formation (Schisto-Calcaire Group), Republic of the Congo, in the Niari-Nyanga and Comba subbasins of the neoproterozoic west Congo basin after the marinoan glaciation event

Anna Perla Ackouala Mfere, Franck Delpomdor, Jean-Noël Proust, Florent Boudzoumou, Yannick y Callec, Alain Préat

Journal Pre-proof

Facies and architecture of the SCIc formation (Schisto-Calcaire Group), Republic of the Congo, in the Niari-Nyanga and Comba subbasins of the neoproterozoic west Congo basin after the marinoan glaciation event

Anna Perla Ackouala Mfere, Franck Delpomdor, Jean-Noël Proust, Florent Boudzoumou, Yannick Callec, Alain Préat

PII: S1464-343X(20)30027-3

DOI: https://doi.org/10.1016/j.jafrearsci.2020.103776

Reference: AES 103776

To appear in: *Journal of African Earth Sciences*

Received Date: 18 December 2018

Revised Date: 24 January 2020

Accepted Date: 24 January 2020

Please cite this article as: Mfere, A.P.A., Delpomdor, F., Proust, Jean.-Noë., Boudzoumou, F., Callec, Y., Préat, A., Facies and architecture of the SCIc formation (Schisto-Calcaire Group), Republic of the Congo, in the Niari-Nyanga and Comba subbasins of the neoproterozoic west Congo basin after the marinoan glaciation event, *Journal of African Earth Sciences* (2020), doi: https://doi.org/10.1016/j.jafrearsci.2020.103776.

Facies and architecture of the SCIc Formation (Schisto-Calcaire Group), Republic of the Congo, in the Niari-Nyanga and Comba subbasins of the Neoproterozoic West Congo Basin after the Marinoan glaciation event

Authors:

Anna Perla Ackouala Mfere[1,2]*, Franck Delpomdor[3], Jean-Noël Proust[4], Florent Boudzoumou[2], Yannick Callec[5], Alain Préat[1]

Affiliations:

[1]*Université Libre de Bruxelles, Department of Earth Sciences and Environmental Sciences, 50 av. FD Roosevelt, B-1050, Brussels, Belgium, Corresponding author: ackouala8@yahoo.fr*

[2]*Université Marien Ngouabi, Département de Géologie BP69, Brazzaville, People's Republic of the Congo*

[3]*Illinois State Geological Survey, University of Illinois at Urbana-Champaign, 615 E. Peabody Dr, US-61820, Champaign, IL, USA*

[4] *Univ Rennes, CNRS, UMR6118 Geosciences, 35000 Rennes, France*

[5]*Bureau de Recherches Géologiques et Minières, 3 av. Claude Guillemin, BP 36009, F-45060 Orléans, Cédex2, France*

Keywords: Neoproterozoic, West Congolian Supergroup, Facies, Sequence stratigraphy, Basin evolution

Abstract

The Neoproterozoic Schisto-Calcaire Group (630 to ca. 580 Ma) was deposited on an extensive carbonate shelf in the margin of the Congo Craton in the Niari-Nyanga and Comba subbasins (Gabon and Republic of the Congo). It consists of three carbonate-dominated subgroups (SCI to SCIII, up to 1300 m-thick) recording relative sea-level changes. The SCI_c Formation, at the upper part of the SCI Subgroup, is a carbonate succession of meter-scale shallowing-upward cycles, composed of a standard sequence of 7 facies grouped in 5 facies associations recording the evolution of a marine ramp from distal carbonate muds and giant stromatolitic bioherms (F1-F2) and extensive ooid shoals (F3), to

proximal settings submitted to evaporation near a sabkha (F7). Fifth-order 'meter-scale' (or elementary parasequences) packages are grouped into fourth-order sequences (parasequence sets), which are not correlative in the whole basin. Two categories of fifth-order elementary parasequences are recognized, on the basis of physical bounding surfaces: (i) subtidal cycles bounded by marine flooding surfaces across which subfacies deepen; and (ii) peritidal cycles bounded by subaerial exposure surfaces. These cycles are the result of the interplay of relative sea-level changes due to eustatic variations related to periodic extensional tectonic events affecting the whole basin. The Niari-Nyanga and Comba subbasins experienced basin tectonics in the general context of the rifting of Rodinia creating changes of relative sea-level in the different parts of the shelf. The SCI_c cycles are enclosed into a third-order sequence with two major transgressive-regressive phases, related to the deposition of the SCI Subgroup. The most typical sedimentologic feature of the SCI_c Formation is the deposition of giant stromatolitic bioherms (stacked up to 20 m) topped by ooid shoals (up to 75 meters thick) deposited during high systems tract prograding and forced regressive systems tract phases that ended with a lowstand systems tract phase with evaporitic and karstic conditions at the top of the SCI_c Formation. The elementary parasequences and parasequence sets are probably the result of the migration of lateral environments related to the variation of the energy in relation to tectonic setting. As a result, a regional sea-level increase is for the first time highlighted in transgressive systems tract phase (composed of microbial induced sedimentary structures Facies) in the lower part of the SCI_c Formation. The third-order succession can be followed more than 100 km in the Republic of the Congo and several hundred meters from South of Gabon to the Lower Congo in the Democratic Republic of the Congo. Tentative detailed sequence stratigraphy correlations between both Congo's highlight the role of tectonics affecting both areas.

1. Introduction

The Neoproterozoic Era (~1000-540 Ma) was marked by several catastrophic Snowball Earth-type ice ages involving short-lived global climate and eustatic events (Kirchvink, 1992; Hoffman et al., 1998; Hoffman and Schrag, 2002). At least three long-live Neoproterozoic glacioeras (~715-660 Ma Sturtian, ~655-635 Ma Marinoan, and ~583-581 Ma Gaskiers events were widely identified (Young, 1995; Wang and Li, 2003; Allen et al., 2004; Deynoux et al., 2006; Hoffman and Li, 2009; Hoffman et al., 2017). Each event was marked by the deposition of diamictites, widely distributed on all continents. The diamictites are commonly overlain in a sharp contact by a cap carbonate unit, interpreted as the result of a sudden switch back to a greenhouse (Hoffman and Schrag, 2002) climate related to increase of atmospheric carbon dioxide due to volcanic degassing (Hoffman and Schrag, 2002). This latter event caused a rapid post-glacial marine transgression, and the turning on of the carbonate factory.

However, other works have cautioned that diamictites are not unambiguous glacial indicators, but could represent tectonostratigraphic successions formed in tectonically-active rift basins as Rodinia broke apart, thereby demanding caution in directly inferring glacially controlled climatic and eustatic interpretations from such successions (Direen and Jago, 2008; Eyles and Januszczak, 2004; Arnaud and Eyles, 2006; Carto and Eyles, 2012; Delpomdor et al., 2016). In western-central Africa, recent publications have argued that the post-Marinoan carbonate successions record a marine transgression, interconnected with diachronous and regional tectonic processes related to the onset of the pre-collisional magmatic arc in the Araçuaí-West Congo Orogen, dated around 630 Ma, with an orogenic climax around 585-560 Ma (Delpomdor et al., 2016, 2018, 2019).

The aim of our paper is to contribute to the debate on the deposition of carbonate successions in western-central Africa, recording a marine transgression after the Marinoan glaciation event. We propose (1) to re-interpret the deposition of the SCI_c Formation in the Niari-Nyanga and Comba subbasins of the Neoproterozoic West Congo Basin (NWCB), located in the Republic of the Congo, and (2) to describe the vertical thickness variations in the cycles and their organization into different sequence orders as a result of tectonic and eustatic mechanisms. A particular interest concerns the hummocky cross-stratification or « HCS » in the oolitic shoals, which is reported for the first time in this stratigraphic unit. It should also be noted that the oolitic shoals are recently intensively used by the cement industry.

2. Geological Setting

The research area concerns exposures along 1,300 km of the western margin of the Congo Craton, from southwestern Gabon across the Republic of the Congo (RC) to the western part of the Democratic Republic of the Congo (DRC) to northern Angola (Fig. 1). The Pan-African West Congo Belt (WCB) is part of the Araçuaí-West Congo Orogen (AWCO) formed during the Gondwanaland amalgamation (ca. 550 Ma; Pedrosa-Soares et al., 2008). In RC, the WCB is subdivided into the aulacogen foreland and the Mayombe thrust-and-fold belt domains, which differ in deformation style and metamorphic grade. The foreland domain is composed of weakly to unmetamorphosed rocks unlike those of the thrust-and-fold belt domain. The WCB comprises several Neoproterozoic sedimentary subbasins (Tait et al., 2011; Delpomdor and Préat, 2013; Préat et al., 2011, 2018), here unified as the NWCB, which is now divided from north to south into the Niari-Nyanga, Comba, Lower Congo and North Angola subbasins (Fig. 1). The Niari-Nyanga and Comba subbasins in RC

are filled with volcano-sedimentary successions of the West Congolian Supergroup (WCS) (Dadet, 1969; Alvarez and Maurin, 1991; Thiéblemont et al., 2009; Charles et al., 2015; Affaton et al., 2016; Préat et al., 2018). In RC, the lithostratigraphic terminology of the WCS has been recently modified by Charles et al. (2015) with, from base to top: (i) the rift-related volcano-sedimentary Sounda Group, correlated to the ~1000-930 Ma Nzadi and ~920-910 Ma Tshela/Senke Banza groups (including the Inga-Lufu- and Gangila-type bimodal magmatism) in DRC (Baudet et al., 2013), (ii) the passive-margin Mayombe Group, stratigraphic equivalent to the Sansikwa and Haut-Shiloango subgroups in DRC, (iii) the Niari Group formerly called the "Upper Diamictite", (iv) the shallow marine Schisto-Calcaire Group, stratigraphic equivalent to the Lukala Subgroup in DRC, including a carbonate outer shelf with nearshore barriers and evaporitic lagoons, and (v) the late-orogenic Mpioka Group (Fig. 2). The Sounda Group is subdivided into the Nemba, Kakamoéka and Mvouti subgroups; the Mayombe Group includes the Mossouva, Lower Diamictite and Louila/Bouenza subgroups; the Schisto-Calcaire Group comprises the SCI, SCII and SCIII subgroups (Dadet, 1969; Alvarez and Maurin, 1991; Alvarez, 1995; Préat et al., 2018; Fig. 2).

3. Geochronology

The absolute age of the WCB is relatively well constrained. In DRC, the Sansikwa Subgroup, a stratigraphic equivalent to the Mossouva Subgroup of the Mayombe Group in RC, is younger than 920-910 Ma (Tack et al., 2001). The Sansikwa Subgroup is intruded by the Sumbi-type dolerite feeder sills and dykes (De Paepe et al., 1975; Kampunzu et al., 1991). U-Pb determinations on baddeleyite single-grains from a dolerite sill yielded a crystallization age of 694 ± 4 Ma (Straathof, 2011), an age younger than the formerly accepted Sturtian age. The Upper Diamictite Formation in DRC

(stratigraphic equivalent with the Niari Group in RC) is interlayered with basalts of tholeiitic affinity including the Kimbungu pillows and hyaloclastic breccias. In Gabon, zircons from a tuff in the metasedimentary Louila/Bouenza Subgroup yielded a U-Pb SHRIMP age of ≤ 713 ± 49 Ma (Thiéblemont et al., 2009). Detrital zircon geochronology and provenance analysis of the Lower Diamictite Formation from DRC gave a maximum depositional age of ~700 Ma (Muanza-Kant et al., 2016) constraining the episodic extensional activity recorded on the present-day African side of the AWCO. Detrital U-Pb single-zircon analysis from the basal contact of the upper formation of the Haut-Shiloango Subgroup in DRC, stratigraphically equivalent with the Louila/Bouenza Subgroup, points to a maximum depositional age of ~650 Ma (Frimmel et al., 2006). Carbonates of the uppermost Haut-Shiloango Subgroup were probably deposited around 645 Ma, according to near-primary $^{87}Sr/^{86}Sr$ ratios which are similar to carbonates deposited worldwide during this time interval (Frimmel et al., 2006; Poidevin, 2007). Similarly, carbonates of the CII unit of the Lukala Subgroup in DRC, stratigraphic equivalent with the SCII Schisto-Calcaire Group, were deposited around ~575 Ma (Poidevin, 2007). Regional metamorphism of the WCB is constrained by an Ar-Ar age of 566 ± 42 Ma (Frimmel et al., 2006) in good agreement with the ~585-560 Ma orogenic climax of the AWCO in Brazil (Pedrosa-Soares et al., 2011). Late Pan African tectonics are constrained by an Ar-Ar age of 524.6 ± 4.6 Ma on riebeckite in quartz vein in DRC (Tack et al., 2018) and an K-Ar age of 499 ± 19 Ma on illite crystallinity analysis from micas in the Mpioka Group (Fullgraf et al., 2015), that is coeval with 540-490 Ma ages obtained in Angola (Monié et al., 2012).

The SCI_c has never been dated but is younger than the Niari Group that is overlain by the cap carbonates (SCI_a), and is older than the carbonates of the SCII Subgroup of the Schisto-Calcaire Group (Fig. 2).

4. Methodology

Twenty-seven stratigraphic sections were selected in the SCI_c Formation from outcrops along roads, rivers and in the savanna in two key areas of the Niari-Nyanga and Comba subbasins of the NWCB (Fig. 3). The thinnest section is 2 meter-thick and the thickest is 57 meter-thick. Since the sections have been logged and described close to each other, sometimes in places without localities, it has not been possible to name them systematically according to the geographical locations. The 27 sections are named from B to Y (Ackouala Mfere, 2017) with also MAD8016, MAD8018 and MAD8019. The sections A and E belonging to the SCI_b siltstones (Table 1) are not considered here, sections G and MAD8018 are located in active quarries (Sonocc at Loutété), section MAD1016 is located in Bitoto, section MAD8017 is located in an active quarry (Saris quarry, near Nkayi), and section MAD8019 is located near the locality of Zanzo (Fig. 3). The coordinates of the outcrops are summarized in Table 1.

Up to 500 samples were collected for petrography and thin section analysis in order to describe facies associations. The carbonate classification terminologies of Dunham (1962), Embry and Klovan (1972), Sibley and Gregg (1987) were employed for the description of components, matrix and cements. The non-skeletal grains (ooids, intraclasts, peloids, aggregate grains, vadoids), sedimentary textures and structures were systematically quantified.

5. Facies association and depositional model

The carbonates of the Schisto-Calcaire Group (SCI, SCII and SCIII Subgroups) were described by Préat et al. (2018). In this paper, we focus on the SCI_c Formation that we describe and interpret in terms of depositional environments and sequences.

The SCI_c succession contains five facies associations(FA1 to FA5) that are composed of seven facies (F1 to F7) defined by their lithologies, sedimentary structures, textures, fossil contents (microbial mats) and interpreted as deposited in different depositional environments. Facies 3 (F3) is divided into 4 sub-types (F3a,b,c,d) due to the presence of ooids in the mentioned sub-types. These largely marine facies associations are described from the deepest to the shallowest settings and are summarized in Table 2. In this paper, ramp terminology was adopted from Burchette and Wright (1992) with (1) the outer-ramp below the storm wave base (SWB) in the offshore; (2) the mid-ramp between the SWB and the fair-weather wave base (FWWB) in the shoreface transition and (3) the inner-ramp above the FWWB including either high energy shoreface environments and back-shoal infratidal to supratidal environments (e.g., muddy lagoon, tidal flats, swamps) in the backshore.

Outer-ramp

5.1. Facies association 1 (FA1)

Description

FA1 is represented by homogeneous clayey and laminar silty mudstone (F1) (Figs. 4A,C). The laminae consist of a subhorizontal, slightly undulating, alternation of light and darker layers of clayey carbonate siltstones and microbial dome-like (< 0.5 mm) or microlenticular (up to 2.5 mm) mudstones respectively (Figs. 4A-C).

Interpretation

FA1 represents Microbial Induced Sedimentary Structures (MISS; *sensu* Noffke, 2010). The absence of ripple marks, hummocky cross-stratification (HCS), erosional remnants, mat chips, mat curls, true

fenestral fabrics, desiccation cracks and gas domes suggests a quiet and deep environment (40-60 m?) in the photic zone. The environment is typical of the offshore below SWB as for example on the Ordovician continental shelf of the Montagne Noire, France (Noffke, 2000).

Mid-Ramp

5.2. Facies association 2 (FA2)

FA2 includes giant reefal stromatolites with stromatoclast floatstones (F2) and ooid grainstones (F3a with HCS).

Description

F2 displays a variety of domes, columns and cone-shaped morphologies forming bioherms and/or biostromes (Figs. 5A-B and D). Reefs, ranging in sizes from 1 m up to 10 m, are exposed as isolated bodies or stacked in large complexes. Narrow inter-reef areas between the domes, and more commonly between the columns, are filled with stromatoclast floatstones with centimetric-sized and elongated fragments or breccias. F3a consists of grey colored oolite grainstones/packstones overlying F2. HCS with gently curved and low angle cross-laminations (< 10°) and swaley cross-stratifications (SCS) are associated with F3a (Figs. 6D-G). The oolites, ranging between 400 μm and 650 μm in diameter, are spherical, concentric or composite. Monocrystalline calcite or rosettes of former sulphate minerals often replace the nuclei.

Interpretation

The giant dome- and cone-shaped stromatolites formed subaqueously in mid-ramp settings (Kromkamp et al., 2007; Perkins et al., 2007). Stromatoclasts suggest wave- and storm-dominated environments. F2 is locally interstratified and overlain by cross-stratified oolite grainstones of facies 3a (see below, Fig. 6H). HCS in the oolite grainstones (details in section 6.2.) confirms sedimentation between the SWB and the FWWB. Oolites originally formed in shallow water more likely around 2 m deep (Keith and Zuppann, 1993) have been later removed from inner-ramp to the mid-ramp by wave action. Concentrically laminated oolites attest high-energy shoals. HCS are the result of storm action (Walker and Plint, 1992) in the shoreface transition region between SWB and FWWB (Pedersen, 1985; Bose and Chaudhuri, 1990).

Inner-ramp

5.3. Facies association 3 (FA3)

FA3 includes oolite grainstones/packstones (F3a without HCS), floatstones/packstones (F3b) and (dolo)wackestones/(dolo)packstones-grainstones (F3c).

Description

F3a consists of oolitic grainstones/packstones (Fig. 7A) overlying or interfering with the bioherms. F3 shows planar stratifications, low-angle to tabular cross-beddings, asymmetrical current ripples and herringbone cross-beddings (Figs. 6A-B). The oolites are commonly spherical and concentric, between 400 μm and 650 μm in diameter, associated with larger ones (asymmetric cortex) up to 2 mm. Rosettes of sulphate minerals and bipyramidal quartz crystals are present within the oolites.

F3b includes aggregates (infra-mm to cm lumps and grapestones; Figs. 7D-F), intraclasts and oolites floating in a microsparitic matrix. Intraclasts are elongated fragments of mudstones or microbial laminites. Oolites are spherical to subspherical, asymmetric, micritic, and range from 500 μm to 1.5 mm in diameter.

F3c consists of homogeneous mudstones (Fig. 5D) or peloidal laminar wackestones to grainstones (Fig. 5F) with peloids, oolites or proto-oolites. Angular, planar, cross-stratifications and herringbone cross-beddings are common. The mudstone contains pyrite, pseudomorphs of sulphate minerals, organic matter fragments, detrital quartz, feldspars, and micas. Replaced acicular rods and nodules of sulphate (anhydrite relics) are present.

Interpretation

F3a likely formed between 1 to 6 m in water depth and more likely around 2 m-deep (Keith and Zuppann, 1993) in high-energy shoals as attested by the occurrence of concentric oolites. The shoals were later shortly exposed, as indicated by the presence of large asymmetric ooids or vadoids (Beukes, 1983). Evaporite reflux or hypersaline conditions are shown by the growth of sulphate crystals and bipyramidal quartz which are similar to those described by Shukla and Friedman (1981) and by Mamet and Préat (2005). The sedimentary structures in F3a point to waves and tidal currents reworking as attested by cross-beddings, herringbones and asymmetrical ripples (Chakraborty, 2004; Boulvain, 2010).

F3b-c were deposited in low- to moderate-energy shallow waters located behind oolitic barrier complexes (Bathurst, 1971) in the subtidal, intertidal and supratidal lagoonal environments, locally disturbed by storms (Enos, 1983; Tucker et al., 1990). The sediments were submitted to hypersaline conditions as shown by the pseudomorphs of evaporitic minerals.

249

250 *5.4. Facies association 4 (FA4)*

251 FA4 consists of pisoid floatstones (F3d), intraformational conglomerates (F4), laminar detrital

252 mudstones (F5) and stratiform stromatolites (F6).

253

254 Description

255 F3d consists of pisoid floatstones with asymmetric ooids (1.5 to 2 mm in diameter), peloids

256 and remains of microbial mats (Figs. 9A,D). The pisoids (2 mm to 5 cm in diameter) are

257 irregular, elongate or oval (Figs. 9B-C). Desiccation cracks, keystone vugs, pseudomorphs

258 after anhydrite (even in the pisoid nucleus) are common. Meniscus and pendular cementation

259 are observed, pointing to the presence of typical beach-rock. Intensive fragmentation formed a

260 breccia (F4).

261 F4 is a stratified conglomerate including micritic and centimetric intraclasts with rare 'ghosts'

262 of ooids giving a characteristic ''puzzle'' texture. Spiny and half moonlike oolites are

263 common. Desiccation cracks, calcitized laths or nodules of anhydrite and authigenic

264 bipyramidal quartz crystals are regularly observed.

265 F5 is laminar clayey detrital mudstones (Fig. 10) with detrital content up to 30% (dominant quartz and

266 feldspars) with alternations of light-colored laminae (silty fine sand to fine silt) and dark-colored

267 laminae (dominant pyrite). Desiccation-cracks and organic matter fragments are also associated.

268 F6 consists of gently wavy, flat-laminations with domal structures (Figs. 5E-F). Laminae consist of

269 alternation of darker organic-rich (with pyrite framboids) and lighter organic-poor layers. The matrix

270 contains dispersed idiotopic dolomite rhombs (up to 50 µm). The laminae are sometimes slightly

slumped and lenticular, deformed by crystallization of sulphate minerals occurring as microtepees. Fenestral and crinkled fabrics, and near horizontal sheet-cracks associated with vertical mud-crack are common.

Interpretation

FA4, including F3d to F6, represents peritidal environments submitted to periodic emersions. F3d is indicative of vadose conditions on high-energy shoals with development of asymmetric ooids, pendular and meniscus cements during emersion. This environment is similar to the hypersaline supratidal zone in the Persian Gulf characterized by abundant pseudomorphs of anhydrite (Scholle and Kinsman, 1974). F4 represents a low-energy shallow-water upper intertidal to supratidal environments overprinted by episodic subaerial and marine-vadose diagenesis. Such sediments were sporadically subject to evaporation in hypersaline conditions as recorded by the precipitation of sulphates (Shearman, 1963; Kinsmann, 1969), spiny and half-moon ooids (Flügel, 2004). Laminae associated with mud-cracks in F5 point to a low-energy tidal flat environment in an upper intertidal to supratidal setting (Hardie, 1977; Sellwood, 1986; Clough and Goldhammer, 2000). F6 is interpreted as evaporitic-dominated low 'algal' marshes fringing ponds of channeled belts, similar with the Andros Island, particularly along the backslope of the levees and the beach-ridge washovers (Hardie and Ginsburg, 1977).

5.5. Facies association 5 (FA5)

Description

FA5 includes only clayey silty carbonates and dolomudstones (F7). It consists of stratified darkish microparitized dolomicrite matrix with remnants of microbial mats (Figs. 11A-C). Slumping and small-scale folding are observed. Sulphate (anhydrite, gypsum and polyhalite?) minerals are common and consist of lath-shaped and rosette-like aggregates (Figs. 11D-E), enterolithic nodules, veins, collapse breccias and castellated crystals (*sensu* Clark, 1980).

Interpretation

FA5points to an evaporitic peritidal environment (intertidal, temporarily emerged in the supratidal zone), analogous to the recent littoral lagoons or sabkhas formed under warm semi-arid conditions, along the Persian Gulf and the Mediterranean Coast (Patterson and Kinsman, 1981).

5.6. Interpretation of depositional settings (Fig. 12)

The SCI_c Formation was deposited in a shallow ramp setting (*sensu* Burchette and Wright, 1992). It exhibits clayey mudstones, microbial silty mudstones (outer-ramp), stromatolite biohermal, HCS cross-bedded oolitic packstones/grainstones (mid-ramp) and vadose oolitic grainstones with homogeneous wackestones and laminar microbial bindstones, capped by evaporate dolomudstones (inner-ramp). The sediments were submitted to hypersaline conditions as shown by the abundant pseudomorphs of evaporitic minerals.

The outer-ramp was a site of accumulation of terrigenous clay, silt and carbonate mud with microbial MISS colonization in the quiet waters of the upper offshore at a depth of around 50 meters (FA1). The most common mid-ramp facies are typical of shoreface transition environments with storm-wave

deposition of HCS oolitic series and giant stromatolites development with inter-reefal stromatoclast accumulations (FA2). The inner-ramp facies are heterogeneous with high-energy environments in oolitic sandy shoals, forming a nearshore variably effective barrier with lenticular units and low energy environments in lagoonal settings behind the barrier. The inner-ramp facies are located above the fair-weather wave base from the high-energy shoal and the low energy back-shoal (FA3) to inter- and supratidal high energy beach proximal backshore environments with vadose cementation (meniscus and pendant cements) and planar microbial mats (FA4) passing laterally to the sabkha environments with hypersaline dolomudstones (FA5).

6. Sequence Stratigraphy

6.1. Analysis of high-frequency cycles

Sequence stratigraphy based on the recognition of sedimentary facies and unconformity surface relationships have provided a predictive framework for the evolutionary history of the SCI_c Formation. The 27 sections (2 m to 57 m-thick) show the repetition of complete and incomplete cm to m-scale sequences. The cyclicity is pervasive throughout the SCI_c Formation and generally easy to identify in the field. Five 'ideal' high-frequency shallowing-up cycles (5^{th} order) are recognized in the SCI_c Formation (Fig. 13 and Table 3); they are grouped in two main categories: (i) D-cycles (with D for 'deep') bounded by marine flooding surfaces, across which facies deepen and (ii) S-cycles (with S for 'shallow') bounded by subaerial exposures.

D cycles (2 m to 20 m-thick) are recognized from the lithological curve when a reset of F1 and/or F2 occurs while S cycles do not contain F1 and/or F2. The D cycles are homogeneous, displaying mainly F1 and F2, their thicknesses are highly variable depending of the growth of the stromatolites up to 20

meters (F2). Evidence for major drowning unconformity in the SCI_c succession is provided by the clay sedimentation associated with the MISS facies (see FA1, above) and by the development of giant stromatolites initiating D1 and D2 cycles. The upper part of D-cycles is related to F6 with or without typical products related to emersion or erosion.

S-cycles are centimetric-decimetric to 5-7 m-thick and show a shallowing-upward evolution, when complete, near subaerial exposure conditions are recorded at their tops. They show evolution from an oolite shoal to exposure surface associated with a sabkha environment: (i) the S1 cycle or 'oolite shoal cycle' starts with F3a-b, (ii) the S2 cycle or 'lagoonal cycle' starts with F3c and (iii) the S3 cycle or peritidal cycle starts with F3d. They contain several surfaces that can be erosive due to the scouring of oolite shoals by currents, frequent in shallow-water carbonates (Tucker and Wright, 1990; Strasser, 2016). The S cycles are rather thinner and heterogeneous with a great variability in their facies composition recording a shallow-water sedimentation sometimes with non-deposition in the supratidal settings exhibiting numerous 'hiatal' surfaces. Their succession records high-frequency relative sea-level changes in the upper part of the shallow shelf.

The stacking pattern of the shallowing-upward D and S m-scale cycles led to the recognition of deepening and shallowing up parasequence sets (fourth-order, see below). Two typical sections (Saris and D sections) are presented here as they allow following the successions of a few cycles (Figs. 14-15; Table 4; Ackouala Mfere, 2017).

The parasequence sets (fourth-order) of both sections (and all others in Ackouala Mfere, 2017) are aggradational and progradational.

The parasequence set package, deduced from the D and Saris section, is also recognized in many other sections in the Niari-Comba subbasins of the NWCB from Zanzo at the East to Soulou at the West,

over more than 80 km (Fig. 3). As in Loutété (Sonocc quarry, Préat et al., 2018), it also consists of the succession of the S1, S2 and S3 elementary cycles forming shallowing-upward packages.

6.2. Sedimentary belts, Flooding (F) vs Forced Regression (FR) surfaces

On the basis of the facies associations, we recognize at least three major successions which are partly, or not entirely, superimposed as their precise succession cannot be specified due to the small thickness of each of the studied sections (< 60 m, average ± 15-20 m). Each succession is characteristic of a part of the ramp system and shows the succession of facies as follows (Fig. 16): ORS (outer-ramp succession) with FA1, MRS (mid-ramp succession) with FA2, IRS (inner-ramp succession) with FA3-4-5. Each succession is formed by the stacking of meter-scale shallowing-upward 5^{th}-order or high-frequency cycles (Ackouala Mfere, 2017). ORS succession (from W to E; example with sections O, F, D) is generally thin-bedded and grades up into the massive stromatolitic bioherms of the MRS succession (from W to E; sections T, N, P, F, K, H, B and MAD8019). MRS succession, comprising the massive stromatolitic bioherms (e.g., from W to E; sections T, Q) shows oolitic units with HCS. IRS succession consists of thin- to thick-bedded oolitic units (0.5 to 5 m thick) with trough, planar and herringbone cross-laminations and homogeneous lagoonal units (from W to E, mainly in sections MAD8016, O, M, F, H, D, B, MAS8018, MAD8019). Low-angle clinoforms are present suggesting prograding washover oolitic deposits on the stromatolite bioherms (sections P and Q). The interdigitation (not frequent) and the sharp (common) contacts observed in these two profiles between the oolites and the massive bioherms indicate that the oolitic sands migrated partly during, and mainly after, the biohermal growth.

Based on the different sections, IRS succession is the thickest (up to 55 m) and the ORS the thinnest. The latter is probably thicker because, as being made of clays, it is easily weathered and thus good outcrops are rare. The oolitic shoal has varying thicknesses of a few meters up to about a minimum of 30 m (section Q).

Lateral relationships between the three successions and their 4^{th} and 5^{th} order packages can be deduced from sections T, N, P, Q?, F, K, H, D, B, MAD8019 as all these sections exhibit a marine flooding surface, despite the packages they form, are not time constrained:

(i) most of the above mentioned profiles (F, K, H, D, B, MAD8019) have a similar stacking pattern with alternation of meter-scale FA3/FA4. Lateral thickness variations cannot be established as the sections are limited to the outcrop exposure, but it seems that for the thicker sections, the general FA3/FA4 successions exhibit a similar thickness (~20-25 m) except in MAD8016 /MAD8018 with the thickest thicknesses (at least twice or more if compared with the other sections). These alternations are mostly composed of 5^{th} order shallowing-upward S2 and S3-cycles with vadose diagenesis in the pisoid grainstones (see sub-chapter 5.1), these cycles are grouped in 4^{th} order parasequence sets (Ackouala Mfere, 2017);

(ii) thick stacks (at least 30 m, section Q) of amalgamated packstone/grainstone shoal complexes (FA3 *pro parte*) separating distally downdip biohermal stromatolites (FA2 *pro parte*). The dominantly 5^{th} order progradational cycles (S1 cycles) are rather badly preserved due to the wedge-shaped cross-beddings with planar and trough bedforms up to 1 m-thick and numerous inclined discontinuities representing reactivation surfaces during storm-dominated processes (including HCS);

(iii) thin stacks (2-10 m-thick, sections T, F, D, B, MAD8018) of deeper facies assemblages (FA1 and FA2 *pro parte*) with a few D aggradational cycles (subchapter 6.1).

In the different field sections, we recognized two types of erosional surfaces: marine flooding and forced regression surfaces. Marine flooding surfaces ('F' surfaces) are characterized by a sharp deepening upward in the depositional environments from inner to outer ramp deposits (from W to E; sections T, N, P, Q?, F, D, B, MAD8019, in this latter section three repeated flooding surfaces are present; Fig. 16). One of them, being the only continuous surface, correlates laterally over long distances, is interpreted as a transgressive surface (TS surface). Forced regression surface (FR surface) is also recognized in most places. It is marked by an abrupt passage from offshore facies of the outer ramp (FA1) to the shallow-water inner-ramp facies (FA4) (from W to E; sections O and F) with no evidence of extensive subaerial exposure. In most places, the FR surface underlines prograding oolitic shoal deposits. This surface originates from a falling stage of the base level from the offshore to the proximal backshore, which in our succession represents a sea-level fall of a few tens of meters as facies FA1 (± 40-50m deep) is directly covered by facies FA4 (0-10 m deep).

From the detailed analysis of the 27 sections, we propose an 'ideal' or 'virtual' synthetic SCI succession. It starts with section MAD8019 (with three flooding surfaces), overlain by section Q with the thickest oolite shoal above a FR surface (Fig. 16) and covered by section MAD8018 (with the thickest peritidal facies and silty evaporites at the SCII boundary). The oolite shoals and reefal bodies are parallel and accumulated along a W-E 100 km-long regional axis bordering the Archean Congo Craton located in the North. Based on the recently revised geological map and personal information of BRGM (pers. communication, Y. Callec, BRGM) the width of the oolite shoal is about 30-60 km.

7. Discussion

7.1. Distribution of stromatolites in the Niari-Nyanga and Comba subbasins of the NWCB

Giant stromatolitic bioherms are more developed in the eastern part of the studied area while they are rare and thin (less than 1 m) in the western part (Fig. 16) reflecting probably the variation of the accommodation space.

Growth of the main reef builders is affected by a multitude of environmental factors, such as temperature, illumination, turbidity, substrate, and nutrients levels. Many of these factors vary systematically with depth, and this has led to recognition of reefal depth-related zonations in the Phanerozoic rocks (James and Bourque, 1992), and in the early Neoproterozoic series (Bertrand-Sarfati and Moussine-Pouchkine, 1985; Sarkar and Bose, 1992). Alvarez and Maurin (1991) described a NE deepening of the basin with the development of giant stromatolitic bioherms located at the "junction" between the Niari-Nyanga and Comba subbasins of the NWCB (Bertrand-Sarfati and Vicat, 1987; Trompette and Boudzoumou, 1988). Variation of the accommodation space has controlled the shape and the vertical development of the reefs in the SCI_c Formation. Giant stromatolitic bioherms grew during a relative high sea-level where light and oxygen were sufficient to promote the activity of cyanobacteria as shown previously with the stacks of bodies up to 20 m in height. On the contrary, the flat and laminar stromatolites with small domes (< 80 cm) recorded a progradational phase, most likely because limited accommodation space did not permit development of giant stromatolites.

7.2. Evidence of storm events in the carbonates of the SCI_c Formation

The oolitic grainstones-packstones show undulating bedding referred to as HCS (Dott and Bourgeois, 1982; Duke, 1985; Morsilli and Pomar, 2012), indicative of storm events in the shoreface transition as

446 the greatest potential preservation of these structures is between the fair weather- and storm-wave
447 bases, that is a few to several tens of meters (Dott and Bourgeois, 1982; Dumas and Arnott, 2006).
448 These high-energy conditions bring a large amount of sediment into suspension near the sea floor and
449 the mixture of sediment and water oscillates back and forth from shallow to deep waters. Although
450 most oolites form in wave-dominated shallow water shoals (commonly about 2 m), these grains are
451 readily dispersed by storm return currents in deeper water settings.
452 The general successions exposed in the oolite shoals usually reveal an upward transition from HCS to
453 low-angle tabular cross-bedding. This transition reflects an increase in water hydrodynamics and a
454 shallowing up trend from shoreface to beachface environments. Prograding sequences have been
455 documented in many successions with storm effects indicating an upward decrease in water depth
456 (Dott et Bourgeois, 1982), as in an Indian Neoproterozoic ramp (Chakraborty, 2004) and in the
457 Neoproterozoic Bambuí basin of central-eastern Brazil, which lays on top of the same craton with the
458 West Congo units on the other slide of the Atlantic (Uhlein et al., 2019).
459 In the SCI_c Formation, high-energy events are also attested by the elongated stromaclasts (up
460 to 5 cm in length) accumulated in inter-reef areas between the stromatolites. These high-
461 energy events were probably related to episodic storms that formed the HCS in the oolite
462 shoals.
463
464 *7.3. Development of systems tracts*
465 In the absence of time constraints on sequence stratigraphy hierarchy, the key physical
466 bounding surfaces (flooding and forced regression) and the stacking pattern analysis of high
467 frequency cycles (S *vs*. D) help in deciphering the stratigraphic pattern in the basin. The SCI

is interpreted as a single third-order transgressive-regressive sequence which includes a transgressive systems tract (TST) and a highstand systems tract (HST) after the post-Marinoan deglaciation event (Alvarez, 1995). We here interpret the SCI Subgroup as two transgressive-regressive third-order sequences (Fig. 17). In the first sequence, TST sedimentation started with deposition of the 10-12 m-thick cap carbonates (SCI_a) and about 10-15 m-thick of siliciclastic deposits (lower SCI_b). This latter is followed by an HST phase (upper SCI_b, about 135 m-thick) above a maximum flooding surface (MFS). In the second sequence starting with the SCI_c, a lowstand systems tract (LST) is initiated with very shallow water deposits characterized by the alternation of FA3/FA4 with abundant S2 cycles. The LST is overlain by a TS leading to the development of the 'deep' MISS facies (TST). The MFS above the TST is followed by a HST (giant stromatolites). Favorable environmental conditions helped by high accommodation rates after deposition of mud and siliciclastic layers (MISS facies in our case) resulted in growth of giant stromatolites as described in the Proterozoic ramp of Australia (Sami et al., 2000). Stromatolite growth was surely unable to keep pace with initial sea-level rise, resulting in the deposition of mud-dominated sediments (MISS facies), which probably represents a "condensed" interval.

The HST is marked by complete or incomplete aggradational shallowing-upward cycles as shown in Zanzo, B, D, H, K and F sections (Fig. 16). Laterally, the giant stromatolites interfinger with hummocky cross-bedded oolitic grainstones.

In most places, the giant stromatolites are sharply buried by trough cross-bedded oolitic grainstones (S1 cycles) in a forced regression systems tract (FRST) evolving to subtidal and peritidal facies near emersion (S2 and S3 cycles), when reduced accommodation rates

facilitated the accumulation of the shallowest facies. In some sections, interdigitation with lateral pinch-outs between the giant columnar stromatolites (F2) and the oolite shoals (F3) has been observed. They can be followed laterally over a minimum of a few meters, depending on the size of the outcrops. This interdigitation represents a lateral facies change from giant columnar stromatolites to oolite shoals, which also overlay the stromatolites. Thick oolite shoal stacking units, above the FR surface (see sections T, Q) shows that progradation accelerated with time during the FRST probably due to a net fall of sea-level. Sea-level fall could also be recorded in section Q with exposed areas of carbonate sediments, which produced oolite dunes or large-sized lenses (sections Q and R) as a result of tidal processes.

At the transition to SCII, the succession is marked by deposition of silty evaporites and dolomites at the top of MAD8018 section (Fig. 16). These silty evaporites and dolomites represent a LST of the next sequence in the SCII series. (Fig. 17).

7.4. Facies correlations between the Niari-Nyanga and Comba subbasins in RC to the Lower Congo subbasins in DRC

The C3 Formation (SCI_c equivalent in Lower Congo, DRC) about 240 m-thick, dominantly contains light-grey limestones with greenish-grey shales (C3a Member), and massive to crossed-bedded light grey to whitish oolitic and pisoid limestones with thin layers of greenish shales and intraformational conglomerates (C3b Member) (Lepersonne, 1974; Cailteux et al., 2015; Delpomdor et al., 2015, 2019). The standard sequence starts with open marine environments and oolitic shoals passing to restricted peritidal/sabhka environments behind the oolite shoals in a mid- to inner-ramp setting (Delpomdor et al., 2015, 2019). Due to the long distance (around 150 km between the sections in RC

and DRC) and the absence of globally-correlative marker levels in these unfossiliferous series, the current correlation of SCI_b and SCI_c with respectively C2 and C3 series is a quite simplistic useful interpretation; see Fig. 17. For example, the lowermost part of the SCI_b series consisting of marls and marly limestones, locally limestones in the loop of the Niari river (Dadet, 1969), could be coeval with the lowermost part of the C2 Formation (e.g., C2a to C2c members; stratigraphic correlation after Cahen, 1978), while the uppermost part of the C2 Formation (e.g., C2d to C2e members) consisting of calcareous shales, sandy and muddy limestones and limestones (Delhaye and Sluys, 1923; Lepersonne, 1974; Cailteux et al., 2015; Delpomdor et al., 2015) could be coeval with the upper part of the SCI_b Formation, which is mainly constituted of marly limestones and limestones (Dadet, 1969). The lowermost member of the SCI_c series (e.g., SCI_{c-a} Member) could be laterally coeval with the C2f to C2g members of the C2 Formation, which consist of calcareous shales, sandstones and limestones. The C3 Formation, divided into C3a and C3b members (Cailteux et al., 2015) is proposed in this study as coeval with the lower and upper part of the SCI_c series respectively. Correlation from these shallow-water series with multiple shoaling events deduced from the lithologic patterns is therefore difficult and could be improved by using the sequence stratigraphy data of our work in RC and the study of Delpomdor et al. (2015) in DRC. These marine deposits formed in extensive near shore environments during a global transgression related to the probable deglaciation at the end of Snowball Earth. In both areas, the shelf was block-faulted and structured into highs and shallow depressions, creating complex morphologies as suggested by Alvarez and Maurin (1991) in the Niari-Comba area. Our detailed stratigraphic sequence analysis of the Comba aulacogen combined with paleobathymetric data allows correlation of third-order sequence between the two areas (RC and RDC) (Fig. 17). This reveals that the SCI_b is partly related to a TST phase (SCI_a and lower SCI_b in RC or C2a-b members in

DRC) and an HST phase (upper SCI_b in RC or C2c-e members in DRC). The extreme uppermost part of the C2 formation, e.g., C2f to Ce2h members; observation by Sikorski, 1958) in DRC could laterally correspond to facies recording a LST in RC, and the C3a Member to TST and HST recorded in the lowermost part of the SCI_c series in RC, if we consider that the giant stromatolites never described in DRC are included in this formation. After the lowstand to highstand sequence, the oolite shoals (C3b Member) or the uppermost part of the SCI_c is newly reinterpreted as FRST marked by the progradation of oolite shoals evolving to peritidal facies near emersion atop of the SCI_c series and C3 Formation, when reduced accommodation rates facilitated the accumulation of shallowest facies. As suggested by Delpomdor et al. (2015), the top of the C3 Formation has been exposed to erosion/and or karstification suggesting a regional-scale turn off the carbonate factory. In this context, the silty evaporates at the transition SCI-SCII are interpreted as a LST in the next sequence (SCII Formation in RC or C4 in DRC).

However, we interpret the three positive jumps of the Fischer plot present in the C3a2 to C3b2 units (Delpomdor et al., 2015) as probably related to reactivations of the block-faulting observed in the SCI_c Formation, in this case related by flooding surfaces (Fig. 16). Both areas experienced basin tectonics in the general context of a pre-collisional phase creating changes in relative sea-level by reactivation of pre-existing faults. This implies that the parasequence packages are strongly controlled by tectonics and are diachronous on the scale of the whole basin. Our sequence stratigraphic analysis allows for the first time tentative correlation in the Schisto-Calcaire Group and Lukala Subgroup in RC and DRC respectively. Giant stromatolites observed in RC were identified in the lowermost part of the SCIc series, while stromatolitic reefs (10 m long and a few meters width), associated with breccias and oolitic limestones have been found in the C3b Member (Cahen, 1950). Recently, microbial mats have

been identified in the C3a Member in DRC (Delpomdor et al., 2015). As shown previously, water depth is the first-order control on reef growth and morphology. Deep water is essential for development of giant stromatolites but cyanobacteria need also fine grained sand substrate for best development, as shown previously with the MISS of the F1 (Noffke, 2010). Giant domal stromatolites commonly form in deep water settings (Bertrand-Sarfati and Moussine-Pouchkine, 1985; Dill et al., 1986; Glumac and Walker, 2000) while flat morphologies occur in shallow water settings (Arenas and Pomar, 2010; Glumac and Walker, 2000). Water depth was probably higher in the sedimentary areas located in RC than in the DRC as a result of the structuration of this area by tectonic effects during sedimentation. Although the geometry of deposits of the SCI_c Formation is seen as continuous on the southern edge of the Chaillu Massif, Chorowitz et al. (1990) concluded that the Lower Congo/Sangha aulacogen, extended to the Comba aulacogen, shows multiple pull-apart-type tectonic areas constituted of elongated WNW-ESE tilted blocks defined by NE-SW faults. Therefore, the sedimentation records the development of oolite shoals. The development of a cordon of oolitic sands of the C3 Formation in DRC, similar to the SCI_c Formation of RC, may also be inferred on the NW edge of the Kasaï block. The oolitic shoals seem to bypass the NW Kasaï block by the thickening of oolitic limestones (100-200 m in thickness) in Angola (Schermerhorn and Stanton, 1963).

7.5. Origin of cyclicity

Facies analysis led to the recognition of a cyclic pattern in the SCI_c sedimentation. Generally, the recognized cycles exhibit a shallowing-upward trend, as suggested by the vertical facies evolution along the standard sequence. Autocyclic and allocyclic mechanisms can both lead to shallowing-upward cycles (Strasser, 1991). While autocyclic processes operate within the sedimentary basin with

progradation of tidal flat or lateral migration of tidal channels (Satterley, 1996), allocyclic control mechanisms are independent of the depositional processes and include eustatic sea-level fluctuations (Elrick, 1995) or repeated synsedimentary tectonic downfaulting events, e.g., tectonics model proposed by Cisne (1986). Subsidence does not appear to have been constant during deposition of SCI_c Formation over the whole studied area as the SCI_c thicknesses show important variations; rather it was affected by periodic changes. On the other hand, SCI_c cyclic deposition (fourth-order) is not harmonious, and the cycles are difficult to correlate between neighboring sections (less than a few kilometers) despite the overall regressive depositional trend of the stratigraphic interval and the consistent shallowing-upward parasequence trend within the sections.

There are a variable number of elementary parasequences (fifth-order) at each locality suggesting that most are probably the result of migration of local environments due to multiple shoaling events. In this context, these parasequences seem to be autocyclic (Ginsburg, 1971) and represent the typical evolution (migration, erosion, non deposition) of ooid dunes controlled by currents and sea-level fluctuations at very shallow depths. Moreover, accumulation rate variations and diagenesis could also modified the final shapes of the SCI_c stratigraphical data sets. Additionally, several subaerial exposures of the investigated sections and erosional boundaries suggest periodical drops of the relative sea-level followed by renewed transgressions.

Assuming that the autocyclic mechanism originated from aggradational/progradational trends during deposition of the SCI_c Formation, this process suggests a particular factor affecting the Niari-Nyanga and Comba subbasins of the NWCB to drive the changes in the accommodation space. A tectonic control with reactivation of pre-existing faults (leading to multiple episodes of accommodation space changes) may play a role in the origin of these cycles (see below, 6.6.)

600 The fact that D1 cycles are directly overlain by progradational facies suggests that there was no true
601 drowning and they were not associated with a true eustatic sea-level increase. They have been related
602 to local interference by tectonic movement or autocyclic processes. The lateral and vertical
603 variabilities of thickness of the elementary parasequences could be attributed not only to the variable
604 potential of sediment accumulation in the different environments (shoal, back-shoal, tidal channels,
605 lagoon, shoreface) but also to the tectonic context that created the Niari-Comba subbasins of the
606 NWCB. As a result, random processes dominated and blurred the low-amplitude sea-level signal, and
607 the resulting sedimentary records will differ depending on their location in the basin (Strasser, 2016).
608 The sedimentary environments were generally shallow enough to record the several relative sea-level
609 fluctuations (1-5 m) and produced the common observed S-cycles. As no order or regularity in the
610 cycle pattern is observed, as could be expected if orbital forcing was the dominant mechanism, it is
611 highly probable that autocyclic processes (helped or inferred by tectonics) were dominant, in a general
612 tectonic setting with both constant and differential subsidence along various faulted blocks.
613
614 *7.6. Tectonic significance and regional implication*
615 All of the high-order cycles identified in the SCI_c Formation were deposited under conditions of sea-
616 level fluctuations driven by tectono-eustasy, which dominated the late Neoproterozoic.
617 During Neoproterozoic times, several distinct extensional tectonic episodes affected the São
618 Francisco-Congo Craton in the area related to the development of the AWCO (Pedrosa-Soares and
619 Alkmin, 2011). After 660 Ma, a passive margin developed in the WCB with deposition of the
620 Bouenza-Louila Subgroup in RC, the stratigraphic equivalent Haut-Shiloango Subgroup in DRC,
621 followed by respectively the Upper Diamictite Formation and the Lukala Subgroup (Frimmel et al.,

2006; Poidevin, 2007). These movements in the basin reflected pre-Marinoan extensional events (see Pedrosa-Soares and Alkmin, 2011), enhancing tectono-eustatic fluctuations during the pre-, syn- and post-sedimentary deposition (Delpomdor et al., 2015, 2016, 2019). Under these passive margin conditions, the relative eustatic variations in the SCI_c Formation are the consequence of short-time extensional tectonic activities in the whole basin including several sub-events in Central Africa and recorded through the fifth-order D- and S-cycles. Deepening occurred when relative sea-level and/or accommodation space increased due to short-time extensional tectonic activities leading to the drowning of the former inner-ramp areas.

The same cyclicities have been recognized in the C3 Formation in Lower Congo (Delpomdor et al., 2015, 2019). The tectonics was probably related to the breakup of Rodinia which influenced sedimentary processes through tectonic subsidence and sediment supply in a similar way as occurred along opposing paleo-Atlantic and paleo-Pacific margins of Laurentia (Eyles and Januszczak, 2004).

Even if the timing of the series is poorly constrained in order to establish detailed correlations between the lower part of the Schisto-Calcaire Group in SW Gabon (Préat et al., 2010), Lower Congo region (Delpomdor and Préat, 2013) and our studied area, it appears that the SCI_c overlying the reddish calcareous marls and marls (SCI_b Formation) is coeval with the Nsc1c (Préat et al., 2011, 2018), and probably the top of the C2 Formation and with the C3 Formation in Lower Congo region (DRC; Delpomdor et al., 2015). As shown by Delpomdor et al. (2015, 2019) and in our study, this sedimentation exposes mainly shallowing-upward cycles in response to tectono-eustasy occurring in the late Neoproterozoic (Tack et al., 2001; Li et al., 2008; Delpomdor and Préat, 2013). In RC, general sea-level rise did not occur in one continuous phase as highlighted by the recurrence of the D1 cycles in (D, H, Zanzo, F and T sections; Fig. 16), but was probably triggered by the reactivation of regional

block-faulting (see Strasser, 2016 for general consideration) with extensional faults related to the rifting evolution of the Comba aulacogen (see above). The lateral variability in the thickness of the elementary parasequences (Ackouala Mfere, 2017) is therefore attributed not only to the variable potential of sediment accumulation in the different environments but also to synsedimentary tectonics.

8. Conclusions

The SCI_c Formation was formed in a paleoramp setting from quiet water in the outer-ramp (FA1) to very shallow water under hypersaline conditions in the inner-ramp (FA5). Storm events have been recognized by HCS in the oolitic series and by elongate stromaclasts (up to 5 cm in length) accumulated in inter-reef areas between the stromatolitic bioherms (FA2). The SCI_c Formation records LST, TST, HST and FRST successions (Fig. 17) linked to the reactivation of regional block-faulting and is also marked by a regional TS (Fig. 16). The D and S-cycles or elementary parasequences (meter-scale from 0.1 to 20 meters in thickness) are well developed in the carbonate ramp from outer- to inner-settings with dominant S1 cycles in high energy settings and lagoonal S2 cycles in low energy settings. The magnitude of the sea-level change was mostly small (except during the transgression and the forced regression), less than a few meters as deduced from the average of the tidal cycle ticknesses (1-3 m-thick). This produced a random stack of elementary parasequences, as for example where shoals migrated out of main transport path. The LST in the SCI_c Formation is represented by the maximum of progradation of the whole SCI Subgroup, with decreasing circulation and fluctuating salinities, reflected by development of a sabkha environment with dolomudstones and abundant sulphate pseudomorphs (FA5), also pointing to a probable climate change from semi-arid to arid setting. The SCI_c Formation records high-frequency shallowing-upward cycles generated by an

autocyclic mechanism that is likely controlled by tectonic syn-sedimentary extensional faults related to the rifting of the basin. On a broader scale, the recurrent generation of accommodation space was triggered by short-time extensional tectonic activity related to several sub-events in Central Africa. The cyclic succession of the fourth-order parasequences in the SCI_c Formation has been correlated between the studied sections following the general trend. In detail, each section shows a specific evolution, as for example the FR observed in two sections. The stratigraphic package of the SCI_c Formation can be subdivided into two broad 4^{th}-order sequential units: the first one comprises packages of the laminar clayey silty mudstones (MISS facies) and stromatolite bioherms, the second starts with ooid shoals and is terminated by evaporative dolomudstones. This 'binome' formed of packages of elementary parasequences can be traced across the whole shelf, even while it is impossible to trace the individual parasequences and occurs over more than 100 km reflecting the sedimentary filling of the basin, which is probably tectonically driven. The elementary parasequences and their grouping are diachronic, they do not produce a clear stacking pattern, and cannot be used for chronostratigraphy. Their distribution is related to the amount of accommodation space available, which is primarily controlled by differential subsidence among the faulted-blocks. The best correlation across the basin (from Gabon to Angola) is surely the recognition of this 'binome'.

Acknowledgements

We want specially to thank Total Congo for sponsoring of this study carried out in the frame of a mapping project in the Republic of the Congo. We thank also Georges Zaboukis and Francisco Serbeto Ibanez for the thin section production. We acknowledge Scott Elrick (ISGS) for the helpful discussions and improving the English of the manuscript. We thank the reviewer Fabricío Caxito

and the editor Damien Delvaux for their constructive reviews and helpful criticism.

Bibliography

Ackouala Mfere, A.P., 2017. Sédimentologie, Cyclicité et Diagenèse des Carbonates de la Formation du Schisto-Calcaire (SCIc) dans les sous-bassins de Niari-Nyanga et de Comba en République du Congo, PhD thesis, Université Libre de Bruxelles, 265pp.

Affaton, P., Kalsbeek, F., Boudzoumou, F., Trompette, R., Thrane, K., Frei, R., 2016. The Pan-African West Congo belt in the Republic of Congo (Congo Brazzaville): Stratigraphy of the Mayombe and West Congo Supergroups studied by detrital zircon geochronology. Precambrian Res. 272, 185–202. https://doi.org/10.1016/J.PRECAMRES.2015.10.020

Allen, P.A., Leather, J., Brasier, M.D., 2004. The Neoproterozoic Fiq glaciation and its aftermath, Huqf supergroup of Oman. Basin Res. 16, 507–534. https://doi.org/10.1111/j.1365-2117.2004.00249.x

Alvarez, P., Maurin, J.-C., 1991. Evolution sédimentaire et tectonique du bassin protérozoïque supérieur de Comba (Congo) : Stratigraphie séquentielle du Supergroupe Ouest-Congolien et modèle d'amortissement sur décrochements dans le contexte de la tectogénèse panafricaine. Precambrian Res. 50, 137–171. https://doi.org/10.1016/0301-9268(91)90051-B

Alvarez, P., 1995. Evidence for a Neoproterozoic carbonate ramp on the northern edge of the Central African craton: relations with Late Proterozoic intracratonic troughs. Geol. Rundsch. 84, 636-648.

Arenas, C., Pomar, L., 2010. Microbial deposits in upper Miocene carbonates, Mallorca, Spain. Palaeogeogr. Palaeoclimatol. Palaeoecol. 297, 465–485. https://doi.org/10.1016/J.PALAEO.2010.08.030

Arnaud, E., Eyles, C.H., 2006. Neoproterozoic environmental change recorded in the Port Askaig Formation, Scotland: Climatic vs tectonic controls. Sediment. Geol. 183, 99–124. https://doi.org/10.1016/J.SEDGEO.2005.09.014

Bathurst, R.G.C., 1971. Carbonate sediments and their diagenesis, Elsevier, Amsterdam. https://doi.org/10.1016/0016-7185(73)90072-9

Baudet, D., Fernandez, M., Kant-Kabalu, F. & Laghmouch, M., 2013. Carte géologique de la

720 République Démocratique du Congo au 1/500 000- Province du Bas-Congo. Musée royal de
721 l'Afrique centrale, Tervuren, Belgique & Centre de Recherches Géologiques et Minières,
722 Kinshasa, RD Congo, avec une notice explicative de 50p.
723 Bertrand-Sarfati, J., Moussine-Pouchkine, A., 1985. Evolution and environmental conditions of
724 Conophyton-Jacutophyton associations in the Atar dolomite (Upper Proterozoic, Mauritania).
725 Precambrian Res. 29, 207–234. https://doi.org/10.1016/0301-9268(85)90069-5
726 Bertrand-Sarfati, J., Vicat, J.P., 1987. Les stromatolites columnaires du Schisto-Calcaire du
727 Protérozoïque Supérieur du Congo et leur place dans la sédimentation. Bull. Société Géologique
728 Fr. III, 289–298. https://doi.org/10.2113/gssgfbull.iii.2.289
729 Beukes, N.J., 1983. Ooids and oolites of the proterophytic Boomplaas Formation, Transvaal
730 Supergroup, Griqualand West, South Africa, Coated grains. Springer Berlin Heidelberg, Berlin,
731 Heidelberg. https://doi.org/10.1007/978-3-642-68869-0_18
732 Bose, P.K., Chaudhuri, A.K., 1990. Tide versus storm in epeiric coastal deposition: Two Proterozoic
733 sequences, India. Geol. J. 25, 81–101. https://doi.org/10.1002/gj.3350250203
734 Boulvain, F., 2010. Pétrologie sédimentaire des roches aux processus. Ellipses.
735 Burchette, T.P., Wright, V.P., 1992. Carbonate ramp depositional systems. Sediment. Geol. 79, 3–57.
736 Cahen, L., 1950. Le Calcaire de Sekelolo, le Complexe tillitique et la Dolomie rose C1 dans
737 l'Anticlinal de Congo dia Kati (Bas-Congo). Annales du Musée royal du Congo belge, Tervuren,
738 in 8°. Sciences Géologique. 7, 55 pp.
739 Cahen, L., 1978. La stratigraphie et la tectonique du Super- Nd isotope ratios are listed in Table 5.
740 Ages were groupe Ouest-Congolien dans les zones me ´diane et externe calculated following
741 Ludwig (1999). de l'orogène Ouest-Congolien (Pan-Africain) au Bas-Zaïre et dans les régions
742 voisines. Ann. Mus. R. Afr. Centr., 3 Tervuren (Belg.), in-8°, Sci. Géol. 83, p.150
743 Carto, S.L., Eyles, N., 2012. Sedimentology of the Neoproterozoic (c. 580 Ma) Squantum "Tillite",
744 Boston Basin, USA: Mass flow deposition in a deep-water arc basin lacking direct glacial
745 influence. Sediment. Geol. 269–270, 1–14. https://doi.org/10.1016/J.SEDGEO.2012.03.011
746 Chakraborty, P.P., 2004. Facies architecture and sequence development in a Neoproterozoic carbonate
747 ramp: Lakheri Limestone Member, Vindhyan Supergroup, Central India. Precambrian Res. 132,

29–53. https://doi.org/10.1016/J.PRECAMRES.2004.02.004

Charles, N., Callec, Y., Préat, A., Thiéblemont, D., Delpomdor, F., Malounguila, D., Gloanguen, E., Petitot, J., Ackouala, A.-P., Ndiele, B., Mvoula boungou, I., Moebo Boungou, M., 2015. Notice explicative de la carte géologique de la République du Congo à 1/200 000, Feuille Madingou. Editions BRGM, 225 pp.

Cailteux, J.L.H., Delpomdor, F.R.A., Ngoie Ndobani, J.-P., 2015. The Neoproterozoic West-Congo "Schisto-Calcaire" sedimentary succession from the Bas-Congo region (Democratic Republic of the Congo) in the frame of regional tentative correlations. Geol. Belg. 18, 126-146.

Clark, D.., 1980. The diagenesis of Zechstein carbonate sediments. In: Füchtbauer, H., Peryt, T. (Eds.), The Zechstein Basin with Emphasis on Carbonate Sequences. Stuttgart, E. Schweizerbart'sche Verlagbuchandlung. Contrib. to Sedimentol. 9, 16.

Chorowitz, J., Le Fournier, J., Mvumbi, M.., 1990. La Cuvette Centrale du Zaïre: un bassin initié au Protérozoïque supérieur. Contribution de l'analyse du réseau hydrographique. Comptes-Rendus l'Académie des Sci. Paris 331, 349–356.

Cisne, J.L., 1986. Earthquakes recorded stratigraphically on carbonate platforms. Nature 323, 320–322. https://doi.org/10.1038/323320a0

Clough, J.G., Goldhammer, R.K., 2000. Evolution of the Neoproterozoic dolomite ramp complex, Northeastern Brooks range, Alaska. In: Grotzinger, J.P., James, N.P. (Eds.). Carbonate sedimentation and diagenesis in the evolving Precambrian world. Soc. Econ. Paleontol. Mineral. Spec. Publ. 209–241.

Dadet, P., 1969. Notice explicative de la carte géologique de la République du Congo Brazzaville au 1/500000. Mémoire du Bureau de Recherches Géologiques et Minières 40, 103.

Delhaye, F., Sluys,M., 1923. Esquisse géologique du Congo occidentale. Etude du système Schisto-Calcaire, missions géologiques de 1914 et 1918–19. Etablissement Cartographique E. Patesson, Bruxelles-Uccle, 1923–1924.

De Paepe, P., Hertogen, J., Tack, L., 1975. Mise en évidence de laves en coussins dans les faciès volcaniques basiques du massif de Kimbungu (Bas-Zaïre) et implications pour le magmatisme

778 Ouest-Congolien 98, 251–270.
779 Delpomdor, F., Eyles, N., Tack, L., Préat, A., 2016. Pre- and post-Marinoan carbonate facies of the
780 Democratic Republic of the Congo: Glacially- or tectonically-influenced deep-water sediments?
781 Palaeogeogr. Palaeoclimatol. Palaeoecol. 457, 144–157.
782 https://doi.org/10.1016/J.PALAEO.2016.06.014
783 Delpomdor, F., Tack, L., Cailteux, J., Préat, A., 2015. The C2 and C3 formations of the Schisto-
784 Calcaire Group (West Congolian Supergroup) in the Democratic Republic of the Congo: an example
785 of Post-Marinoan sea level fluctuations as a result of extensional tectonisms. J. Afr. Earth Sci. 110, 14-
786 33.
787
788 Delpomdor, F., Préat, A., 2013a. Early and late neoproterozoic c, o and sr isotope chemostratigraphy
789 in the carbonates of west congo and mbuji-mayi supergroups: A preserved marine signature?
790 Palaeogeogr. Palaeoclimatol. Palaeoecol. 389, 35–47.
791 https://doi.org/10.1016/j.palaeo.2013.07.007
792 Delpomdor, F., Préat, A., 2013b. Early and late Neoproterozoic C, O and Sr isotope
793 chemostratigraphy in the carbonates of West Congo and Mbuji-Mayi supergroups: A preserved
794 marine signature? Palaeogeogr. Palaeoclimatol. Palaeoecol. 389, 35–47.
795 https://doi.org/10.1016/J.PALAEO.2013.07.007
796 Delpomdor, F., Van Vliet, N., Devleeschouwer, X., Tack, L., Préat, A., 2018. Evolution and estimated
797 age of the C5 Lukala carbonate-evaporite ramp complex in the Lower Congo region (Democratic
798 Republic of Congo): New perspectives in Central Africa. J. African Earth Sci. 137, 261–277.
799 https://doi.org/10.1016/J.JAFREARSCI.2017.10.021
800 Delpomdor, R.A., 2017. Facies and micromorphology of the Neoproterozoic Upper Diamictite
801 Formation in the Democratic Republic of Congo : new evidence of sediment gravity flow.
802
803 Deynoux, M., Affaton, P., Trompette, R., Villeneuve, M., 2006. Pan-African tectonic evolution and
804 glacial events registered in Neoproterozoic to Cambrian cratonic and foreland basins ofWest
805 Africa. J. Afr. Earth Sci. 46, 397–426.
806 Dill, R.F., Shinn, E.A., Jones, A.T., Kelly, K., Steinen, R.P., 1986. Giant subtidal stromatolites

807 forming in normal salinity waters. Nature 324, 55–58. https://doi.org/10.1038/324055a0
808 Direen, N.G., Jago, J.B., 2008. The Cottons Breccia (Ediacaran) and its tectonostratigraphic context
809 within the Grassy Group, King Island, Australia: A rift-related gravity slump deposit.
810 Precambrian Res. 165, 1–14. https://doi.org/10.1016/J.PRECAMRES.2008.05.008
811 Dott, R.H., Bourgeois, J., 1982. Hummocky stratification: Significance of its variable bedding
812 sequences. Geol. Soc. Am. Bull. 93, 663. https://doi.org/10.1130/0016-
813 7606(1982)93<663:HSSOIV>2.0.CO;2
814 Duke, W.L., 1985. Hummocky cross-stratification, tropical hurricanes, and intense winter storms.
815 Sedimentology 32, 167–194. https://doi.org/10.1111/j.1365-3091.1985.tb00502.x
816 Dumas, S., Arnott, R.W.C., 2006. Origin of hummocky and swaley cross-stratification— The
817 controlling influence of unidirectional current strength and aggradation rate. Geology 34, 1073.
818 https://doi.org/10.1130/G22930A.1
819 Dunham, R.J., 1962. Classification of Carbonate Rocks According to Depositional Textures 38, 108–
820 121.
821 Elrick, M., 1995. Cyclostratigraphy of Middle Devonian Carbonates of the Eastern Great Basin,
822 Journal of Sedimentary Research. SEPM 65 (1), 61-67
823 Embry, A.F., Klovan, J.E., 1972. Absolute water depth limits of Late Devonian paleoecological zones.
824 Geol. Rundschau 61, 672–686. https://doi.org/10.1007/BF01896340
825
826 Enos, P., 1983. Shelf Environment: Chapter 6. Amer. Ass. Pet. Geol. Stud. Geol. 43, 267–295.
827
828 Eyles, N., Januszczak, N., 2004. “Zipper-rift”: a tectonic model for Neoproterozoic glaciations during
829 the breakup of Rodinia after 750 Ma. Earth-Science Rev. 65, 1–73.
830 https://doi.org/10.1016/S0012-8252(03)00080-1
831 Flügel, E., 2004. Microfacies of Carbonate Rocks. Analysis, Interpretation and Application, Berlin,
832 Heidelberg, New York: Springer-Verlag. Cambridge University Press.
833 https://doi.org/10.1017/S0016756806221940
834 Frimmel, H.E., Tack, L., Basei, M.S., Nutman, A.P., Boven, A., 2006. Provenance and

chemostratigraphy of the Neoproterozoic West Congolian Group in the Democratic Republic of Congo. J. African Earth Sci. 46, 221–239. https://doi.org/10.1016/j.jafrearsci.2006.04.010

Ginsburg, R.N., 1971. Landward Movement of Carbonate Mud: New Model for Regressive Cycles in Carbonates. Amer. Ass. Pet. Geol. Stud. Geol. 55 (2), 340. https://doi.org/10.1306/5D25CE81-16C1-11D7-8645000102C1865D

Glumac, B., Walker, K.R., 2000. Carbonate Deposition and Sequence Stratigraphy of the Terminal Cambrian Grand Cycle in the Southern Appalachians, U.S.A. J. Sediment. Res. 70, 952–963. https://doi.org/10.1306/2DC40943-0E47-11D7-8643000102C1865D

Hardie, L.A., 1977. Sedimentation on the Modern Carbonate Tidal Flats of north- west Andros Island, Bahamas. Johns Hopkins University Press, 202 pp.

Hoffman, P.F., Kaufman, A.J., Halverson, G.P., Schrag, D.P., 1998. A Neoproterozoic snowball Earth. Sciences 281, 1342-1376.

Hardie, L.A., Ginsburg, R.N., 1977. Layering; the origin and environmental significance of lamination and thin bedding. In: Sedimentation on the Modern Carbonate Tidal Flats of Northwest Andros Island, Bahamas (Ed. L.A. Hardie), John Hopkins University, Stud. Geol 22, 50–123.

Hoffman, P.F., Schrag, D.P., 2002. The snowball Earth hypothesis: testing the limits of global change. Terra Nov. 14, 129–155. https://doi.org/10.1046/j.1365-3121.2002.00408.x

James, N.P., Bourque, P.-A., 1992. Reefs and mounds. In: Walker, R.G., James, N.P. (Eds.), Facies Models, Response to Sea Level Change. Geol. Assoc. Canada 1, 323–347.

Kampunzu, A.B., Kapenda, D., Manteka, B., 1991. Basic magmatism and geotectonic evolution of the Pan African belt in central Africa: Evidence from the Katangan and West Congolian segments. Tectonophysics 190, 363–371. https://doi.org/10.1016/0040-1951(91)90438-X

Keith, B.D., Zuppann, C.W. (eds)., 1993. Mississippian oolites and modern analogs. Amer. Ass. Pet. Geol. Stud. Geol. 35, 265 pp. https://doi.org/10.1306/St35571

Kinsmann, D.J.J., 1969. Modes of formation, sedimentary associations and diagnostic features of shallow-water and supratidal evaporites. Bull. Am. Assoc. Petrol. Geol. 53, 830–840.

Kirschvink, J.L., 1992. Late Proterozoic low-latitude global glaciation: the snowball Earth. In: Schopf,

J.W., Klein, C., (eds), The Proterozoic biosphere: a multidisciplinary study. Cambridge University Press, Cambridge, 51-52.

Kromkamp, J.C., Perkins, R., Dijkman, N., Consalvey, M., Andres, M., Reid, R.P., 2007. Resistance to burial of cyanobacteria in stromatolites. Aquat. Microb. Ecol. 48, 123–130. https://doi.org/10.3354/ame048123

Lepersonne, J., 1974. Carte géologique à l'échelle 1/200000. Notice explicative de la feuille Ngungu (Degré carré S6/14 = SB 33.9). République Démocratique du Congo. Département des Mines, Direction du Service Géologique, 61 pp.

Li, Z.X., Bogdanova, S.V., Collins, A.S., Davidson, A., De Waele, B., Ernst, R.E., Fitsimons, I.C.W., Fuck, R.A., Gladkochub, D.P., Jacobs, J., Karlstom, K.E., Lu, S., Natapov, L.M., Pease, V., Pisarevsky, S.A., Thrane, K., Vernikovsky, V., 2008. Assembly, configuration, and break-up history of Rodinia: a synthesis. Precambrian Research 160 (1–2), 179–210.

Mamet, B., Préat, A., 2005. Sédimentologie de la série viséenne d'Avesnes-sur-Helpe (Avesnois, Nord de la France). Geol. Belgica 8, 91–107.

Monié, P., Bosch, D., Bruguier, O., Vauchez, A., Rolland, Y., Nsungani, P., Buta, N.A., 2012. The late Neoproterozoic/early palaeozoic evolution of the West Congo belt of NW Angola: geochronological (UPb and Ar-Ar) and petrostructural constraints. Terra Nova 24 (3), 1-10.

Morsilli, M., Pomar, L., 2012. Internal waves vs. surface storm waves: a review on the origin of hummocky cross-stratification. Terra Nov. 24, 273–282. https://doi.org/10.1111/j.1365-3121.2012.01070.x

Muanza-Kant, P., Mpiana, Ch, Kanda-Nkula, V., Tack, L., Baudet, D., Archibald, D.B., Glorie, S., 2016. The lower Diamictite Formation of the Cataractes Group, West Congo Supergroup (Bas-Congo, DRC): a 700 Ma marker of extensional episodic activity during breakup of Columbia., in: 5th International Geologica Belgica 2016 Congress, 26-29 January 2016. University of Mons, Mons, Belgium, P. 57. Abstract Book.

Noffke, N., 2010. Geobiology: Microbial mats in sandy deposits from the Archean era to today. Springer. https://doi.org/10.1007/978-3-642-12772-4

892 Noffke, N., 2000. Extensive microbial mats and their influences on the erosional and depositional
893 dynamics of a siliciclastic cold water environment (Lower Arenigian, Montagne Noire, France).
894 Sediment. Geol. 136, 207–215. https://doi.org/10.1016/S0037-0738(00)00098-1
895 Patterson, R.J., Kinsman, D.J.J., 1981. Hydrologic Framework of a Sabkha Along Arabian Gulf. Am.
896 Assoc. Pet. Geol. Bull. 65, 1457–1475.
897
898 Pedersen, G.K., 1985. Thin, fine-grained storm layers in a muddy shelf sequence: an example from the
899 Lower Jurassic in the Stenlille 1 well, Denmark. J. Geol. Soc. London. 142, 357–374.
900 https://doi.org/10.1144/gsjgs.142.2.0357
901 Pedrosa-Soares, A.C., Alkmim, F.F., Tack, L., Noce, C.M., Babinski, M., Silva, L.C., Martins-Neto,
902 M.A., 2008. Similarities and differences between the Brazilian and African counterparts of the
903 Neoproterozoic Araçuaí-West Congo orogen. Geol. Soc. London, Spec. Publ. 294, 153–172.
904 https://doi.org/10.1144/SP294.9
905 Pedrosa-Soares, A.C., Alkmin, F.F., 2011. How many rifting events preceded the develop- ment of the
906 Araçuai–West Congo orogen? Geonomos 19 (2), 244–251.
907 Pedrosa-Soares, A.C., Babinski, M., Noce, C., Martins, M., Queiroga, G., Vilela, F., 2011. Chapter 49
908 The Neoproterozoic Macaúbas Group, Araçuaí orogen, SE Brazil. Geol. Soc. London, Mem. 36,
909 523–534. https://doi.org/10.1144/M36.49
910 Perkins, R.G., Kromkamp, J.C., Pamela Reid, R., 2007. Importance of light and oxygen for
911 photochemical reactivation in photosynthetic stromatolite communities after natural sand burial.
912 Mar. Ecol. Prog. Ser. 349, 23–32. https://doi.org/10.3354/meps07087
913 Poidevin, J.L., 2007. Stratigraphie isotopique du strontium et datation des formations carbonatées et
914 glaciogéniques néoprotérozoiques du Nord et de l'Ouest du craton du Congo. Comptes Rendus -
915 Geosci. 339, 259–273. https://doi.org/10.1016/j.crte.2007.02.007
916 Préat, A., Delpomdor, F., Ackouala Mfere, A.P., Callec, Y., 2018. Paleoenvironments, δ13C and δ18O
917 signatures in the Neoproterozoic carbonates of the Comba Basin, Republic of Congo:
918 Implications for regional correlations and Marinoan event. J. African Earth Sci. 137, 69–90.
919 https://doi.org/10.1016/j.jafrearsci.2017.09.002

Préat, A., Kolo, K., Prian, J.-P., Delpomdor, F., 2010. A peritidal evaporite environment in the Neoproterozoic of South Gabon (Schisto-Calcaire Subgroup, Nyanga Basin). Precambrian Res. 177, 253–265. https://doi.org/10.1016/J.PRECAMRES.2009.12.003

Préat, A.R., Delpomdor, F., Kolo, K., Gillan, D.C., Prian, J.-P., 2011. Stromatolites and Cyanobacterial Mats in Peritidal Evaporative Environments in the Neoproterozoic of Bas-Congo (Democratic Republic of Congo) and South Gabon. Springer, Dordrecht, pp. 43–63. https://doi.org/10.1007/978-94-007-0397-1_3

Sarkar, S., Bose, P.K., 1992. Variations in Late Proterozoic stromatolites over a transition from basin plain to nearshore subtidal zone. Precambrian Res. 56, 139–157. https://doi.org/10.1016/0301-9268(92)90088-6

Satterley, A.K., 1996. The interpretation of cyclic successions of the Middle and Upper Triassic of the Northern and Southern Alps. Earth-Science Rev. 40, 181–207. https://doi.org/10.1016/0012-8252(95)00063-1

Scholle, P.A., Kinsman, D.J.J., 1974. Aragonitic and High-Mg Calcite Caliche from the Persian Gulf--A Modern Analog for the Permian of Texas and New Mexico. J. Sediment. Res. 44, 904–916. https://doi.org/10.1306/212F6BD6-2B24-11D7-8648000102C1865D

Sellwood, B.W., 1986. Shallow-marine carbonate environ- ments. In: H.G. Reading (Editor), Sedimentary Environ- ments and Facies. Blackwell, 2nd ed. 283 342.

Shearman, D.J., 1963. Recent anhydrite, gypsum, dolomite and halite fromthe coastal flat of the Arabian shore of the Persian Gulf. Proc. Geol. Soc. Lond. 1607/63, 5

Schermerhorn, L.J.G., Stanton, W.I., 1963. Tilloids in the West Congo geosyncline. Q. J. Geol. Soc. 119, 201–241. https://doi.org/10.1144/gsjgs.119.1.0201

Shukla, V., Friedman, G.M., 1981. An unusual occurrence of surficial anhydrite in a moist temperate zone: Example from the Lockport Formation (Middle Silurian) of New York. Sediment. Geol. 29, 125–131. https://doi.org/10.1016/0037-0738(81)90003-8

Sibley, D.F., Gregg, J.., 1987. Classification of Dolomite Rock Textures. J. Sediment. Res. Vol. 57, 967–975. https://doi.org/10.1306/212F8CBA-2B24-11D7-8648000102C1865D

Sikorski, J., 1958. Echelle stratigraphique provisoire des étages C1-C2-C3 du système Schisto-Calcaire du Bas-Congo. CIMINGA, note n°15.

Straathof, G.B., 2011. Neoproterozoic low latitude glaciations: an african perspective. The University of Edinburgh.

Strasser, A., 2016. Hiatuses and condensation: an estimation of time lost on a shallow carbonate platform. Depos. Rec. 1, 91–117. https://doi.org/10.1002/dep2.9

Strasser, A., 1991. Lagoonal-peritidal sequences in carbonate environments: autocyclic and allocyclic processes. In: Einsele G, Ricken W, Seilacher A (Eds), Cycles and events in stratigraphy. Springer, Berlin, 709–721.

Tack, L., Wingate, M.T.., Liégeois, J.-P., Fernandez-Alonso, M., Deblond, A., 2001. Early Neoproterozoic magmatism (1000–910 Ma) of the Zadinian and Mayumbian Groups (Bas-Congo): onset of Rodinia rifting at the western edge of the Congo craton. Precambrian Res. 110, 277–306. https://doi.org/10.1016/S0301-9268(01)00192-9

Tack, L., De Grave, J., Burgess, R., Baudet, D., Fernandez-Alonso, M., Kongota-Isasi, E., Nseka-Mbemba, P., Delvaux, D., 2018. 525 Ma riebeckite in a quartz vein into the Noqui granite: evidence for a late Pan African extensional event in the West Congo Belt (Matadi area, Bas-Congo region, DR Congo)**.** 17th Conference of the Geological Society of Africa and 27th Colloquium of African Geology. Aveiro, Portugal.

Tait, J., Delpomdor, F., Preat, A., Tack, L., Straathof, G., Nkula, V.K., 2011. Chapter 13 Neoproterozoic sequences of the West Congo and Lindi/Ubangi Supergroups in the Congo Craton, Central Africa. Geol. Soc. London, Mem. 36, 185–194. https://doi.org/10.1144/M36.13

Thiéblemont, D., Castaing, C., Billa, M., Bouton, P., Préat, A., 2009. Notice explicative de la carte géologique et des ressources minérales de la République Gabonaise à 1/1000000. Program. Sysmin 8 ACP GA 017 384pp.

Trompette, R., Boudzoumou, F., 1988. Palaeogeographic significance of stromatolitic buildups on

Late Proterozoic platforms: The example of the West Congo basin. Palaeogeogr. Palaeoclimatol. Palaeoecol. 66, 101–112. https://doi.org/10.1016/0031-0182(88)90083-1

Tucker, M.E., Wright, V.P., Dickson, J.A.D., Wiley InterScience (Online service), 1990. Carbonate sedimentology. Blackwell Scientific Publications.

Tucker, M.E., Wright, V.P., 1990. Carbonate Sedimentology. Blackwell Scientific Publications, Oxford, 482 pp.

Uhlein, G.J., Uhlein, A., Pereira, E., Caxito, F.A., Okubo, J., Warren, L. V., Sial, A.N., 2019. Ediacaran paleoenvironmental changes recorded in the mixed carbonate-siliciclastic Bambuí Basin, Brazil. Palaeogeogr. Palaeoclimatol. Palaeoecol. 517, 39–51. https://doi.org/10.1016/j.palaeo.2018.12.022

Walker, R.G. and Plint, A.G., 1992. Wave-and Storm-Dominated Shallow Marine Systems. In: Walker, R.G. and James, N.P., Eds., Facies Models: Response to Sea Level Change. Geol. Assoc. Canada, Newfoundl. 219–238.

Wang, J., Li, Z.-X., 2003. History of Neoproterozoic rift basins in South China: implications for Rodinia break-up. Precambrian Res. 122, 141–158. https://doi.org/10.1016/S0301-9268(02)00209-7

Young, G.M., 1995. Are Neoproterozoic glacial deposits preserved on the margins of Laurentia related to the fragmentation of two supercontinents? Geology 23, 153. https://doi.org/10.1130/0091-7613(1995)023<0153:ANGDPO>2.3.CO;2

Table 1 Location (latitude, longitude and elevation) of the identified outcrops in the studied area. Most of the outcrops have been described in this study. See Fig. 1, Fig. 16 and text for details.

Table 2 Summary of facies associations (FA) and facies (F) defined in the SCI_c Formation with descriptions and environmental interpretations.

Table 3 Cycle features of SCI_c Formation in the studied area.

Table 4 Detailed description of D and Saris sections

Figure 1 Location map of the Neoproterozoic West Congo Basin (NWCB) divided into Niari-Nyanga, Comba, Lower Congo and North Angola (NA) subbasins. The Niari-Nyanga, Lower Congo and North Angola subbasins record sedimentation on a passive margin of the Congo Craton, and the Comba subbasin belongs to the SE margin of the Sangha aulacogen.

Figure 2 Comparative lithostratigraphy between the West Congolian Supergroup in RC and the West Congo Supergroup in DRC. In RC, the stratigraphy of the West Congolian Supergroup has been recently revised by Charles et al. (2015). In DRC, the Lukala Subgroup, formerly Schisto-Calcaire Subgroup, is divided into five formations (C1 to C5), which are stratigraphically equivalent with the SCI Formation – correlated with the C1 to C3 formations of Lower Congo subbasin, SCII Formation – correlated with the C4 Formation of Lower Congo subbasin, and SCIII Formation – correlated with the C5 Formation of Lower Congo subbasin. Sr is based on worldwide $^{87}Sr/^{86}Sr$ composition of seawater during the Neoproterozoic (1000-542 Ma) Era.

Figure 3 Simplified geological map showing location of the identified outcrops (L1, U and T to Zanzo, V, W and X from East to West). No sections have been described for A, E, L1, U, V, W, X and Y in this study. See Fig. 16 for description of each section.

Figure 4 Field and thin-section photographs of homogeneous clayey mudstones and laminar silty mudstones (F1) in the SCI_c Formation. **(A)** Alternations of darker and purplish layers consisting of clayey silty carbonates and microbial mudstones overlain by a domal stromatolite (in the background). The domal stromatolite represents the lower part of a complex zone of giant stromatolites (15-20 m in height), section D. **(B, C, D)** Planar and undulating platy limestones (3-5 cm-thick) showing alternations of homogeneous carbonate muds and slightly laminar silty mudstones identified as MISS (Microbial Induced Sedimentary Structures) by petrographic description, D and O sections. **(E)** Microbial mats (dark laminations or MISS undulating levels) within a fine microsparitic matrix. Quartz, feldspars and pyrite are recognized within the matrix or overlie the microbial mats, section D. **(F)** Dark bacterial filament in a microsparitic matrix, section D.

Figure 5 Field photographs of the stromatolitic facies (F2 and F6) in the SCI_c Formation. **(A)** Upper part of a giant domal stromatolite with 4-5 m in width, section H. **(B)** Columnar stromatolite with parallel columns, section P. **(C)** Centimetric alternations of grey planar microbial mats and accumulations of coarse-grained stromatoclasts forming radial-bundles, section F. **(D)** Giant "cigare" or coned-shaped stromatolite (10- 15 m in length), section F . **(E)** Wavy and planar microbial mats, section M . **(F)** Small domal stromatolite overlying or laterally relayed by planar microbial mats, section D. **(G)** Succession of domal stromatolites in the top of a stromatolitic bioherm (15-20 m in height), section H.

Figure 6 Sedimentary features of the oolite grainstones in the SCI_c Formation. **(A)** Bidirectional low-angle planar laminations with low-angle truncations, section I. **(B)** Sets of trough-stratifications,

section I. **(C)** Mega-ripples, cross-laminations showing herringbone stratifications, section C. **(D)** Mega-ripples showing hummocks and swales with low-angle laminations, section C. **(E)** Mega-ripples with hummocks (see arrow) showing SCS when the top of the hummocks has been eroded. Stylolites (lower part of the picture) are well developed, with high amplitude, as is generally the case in all the oolitic grainstones, section I. **(F, G)** HCS with furrows showing flat (less) and hollow (more) bottoms passing in the upper part to mega-ripples (cross-laminations), section S. **(H)** Oolite grainstones (F3a) overlying columnar stromatolites (F2), irregular contact between F3a and F2 with thick oolite beds overlying giant stromatolite, section T.

Figure 7 Thin-section and field photographs of the oolitic grainstones-floatstones (F3a and F3b) in the SCI_c Formation**. (A)** Grainstone showing well-sorted spherical oolites (F3a) with both concentric and radial structures. Cementation consists of isopachous lamellar calcite and blocky calcite, section MAD8017. **(B)** Well represented cementation filling the intergranular porosity in an oolite grainstone (F3a). As described later, the cementation consists of isopachous lamellar calcite and a blocky calcite, section MAD8018. **(C)** Asymmetric oolite with a concentric cortex and coarse-grained slightly rosette-like nuclei, section I. **(D)** Greyish floatstone with dominant aggregates, see (F) for facies description, section MAD8018. **(E)** Part of centimetric grapestone in a floatstone ooid-aggregate (F3b), the grapestone consists of micritized ooids bounded together by a microsparitic matrix, section I. **(F)** Millimetric aggregates in a floatstone or 'false' rudstone, see (D) for the field photograph, section I. **(G)** Asymmetric oolites (see black arrows) in a grainstone with equant calcite, section MAD8017. **(H)** Asymmetric oolite (see black arrow) in a grapestone. The asymmetric oolite appears to be reworked before bounded with other oolites to build the grapestone, as shown by the orientation,

section MAD8017.

Figure 8 Thin-section and field photographs of lagoonal facies (F3c) and intraformational conglomerate (F4) in the SCI_c Formation. **(A)** Peloidal grainstone-packstone with micritic oolites and relics of larger oolites exhibiting a fine concentric structure in the outer part of the cortex, section MAD8018. **(B**) Peloidal packstone without micritic oolites or larger concentric oolites as described previously**,** section MAD8018. **(C and E)** Homogeneous mudstone with pyrite and oxidized organic matter relics (see arrow in C), section MAD8016. **(D)** Succession of centimetric beds of greyish homogeneous mudstones, section MAD8019. **(F)** Peloidal grainstone showing herringbone cross-stratifications, top of Saris Section (MAD8017). **(G)** Intraformational conglomerate showing elongated mud-clasts and oolites relics with vadose cementation, section B. **(H)** Intraformational conglomerate with plurimillimetric and inframillimetric mud-clasts. The larger ones are elongated and affected by vertical cracks, section MAD8017.

Figure 9 Thin-section and field photographs of peritidal facies (F3d, F4 and F6) in the SCI_c Formation. **(A)** Reddish floatstone with abundant pisoids, Sonocc section. See (B) and (C) for the microfacies description. **(B, C)** Plurimillimetric pisoids showing a fine concentric structure, the nucleus is micritic and partly replaced by a coarse calcite (B) and consists of oolites (C). **(D)** Millimetric asymmetric oolites oriented in opposite directions in a pisoid floatstone. The asymmetric oolites show a concentric cortex with a coarse granular calcite nucleus, Sonocc section. **(E)** Inframillimetric alternations of planar microbial mats and peloid packstone. Note that peloids (in the lower part) show circular cracks, Sonocc section. **(F)** Calcitized anhydrite rosette in a peloidal

bindstone, MAD8017 section. **(G)** Parts of centimetric mud-clasts interlayered by microbial mats relics, MAD8017 section. **(H)** Spiny (left) and half-moon oolites (right) in a floatstone intraformational conglomerate with abundant micritic oolites, MAD8017 section.

Figure 10 Thin-section and field photographs of the fine-grained laminar detrital mudstones (F5) in the SCI_c Formation. **(A)** Pluricentimetric alternations of grey-light oolite grainstones (F3a) and fine-grained laminar detrital mudstones (F5), section F. **(B)** Fine-grained laminar detrital mudstones (F5) topped by a brecciated bindstone microbial mats (F6) showing random stromatoclasts building slightly radial bundles structures, section J. **(C)** Thin low-angle light-colored laminae (silty fine sand to fine silt) interlayered by dark-colored laminae. Light-colored laminae are enriched in quartz, feldspars, clays minerals, calcite and dolomite crystals (see D). Dark-colored laminae display a pyrite-rich homogeneous mudstone, section F. **(D)** Quartz, feldspars, clinochlore (greenish crystal), pyrite and xeno-to hypidiotopic calcite and dolomite crystals in a light-colored laminae of F5, section F.

Figure 11 Thin section and field photographs of the evaporative dolomudstones (F7) in the SCI_c Formation. **(A, B and C)** Reddish and yellowish dolomudstone with abundant rosettes and laths of evaporative minerals, top of Sonocc section. See Figs. D to G for the microfacies description**. (D and E)** Rosettes and laths of anhydrite now calcitized, the matrix is a slightly microsparitized dolomudstone**. (F)** Nodule of well-preserved anhydrite partly silicified**. (G)** Evaporative dolomudstone showing abundant fenestrae testifying vadose conditions.

Figure 12 Revised sedimentary model of the SCI_c Formation in the Niari-Nyanga and Comba sections of the NWCB in RC from outer-ramp with MISS (FA1) to supratidal sabkha (FA5). Facies associations (FA1 to FA5) represent the standard sequence of the studied formation (see Table 2 for explanation). The previous sedimentary model has been described in Préat et al. (2018).

Figure 13 Types of cycles (D *vs* S) with their facies (F1-F7) successions in the SCI_c Formation, showing shallowing upward trends.'D4 is for 'Deep cyles', 'S' is for Shallow cycles'. See Table 3 for explanation

Figure 14 Stratigraphic section of the active Saris (MAD8017) quarry exposing the SCI_c Formation, showing sample location (8017-1 to 8017-22), lithologic curve (from F1 to F7 facies), sedimentological features and stacking patterns. Explanations in text, for location see Fig. 1. FAS= facies successions, PSQ= parasequence, PSQS= parasequence set, Prog. = progradation, Aggr. = aggradation. M = mudstone, W = wackestone, P = packstone, G = grainstone, R = rudstone, B = boundstone.

Figure 15 Stratigraphic section of the inactive D quarry exposing the SCI_c Formation, sample location (D1 to D85), lithologic curve (from F1 to F7 facies), sedimentological features and stacking patterns. Explanations in text, for location see Fig. 1. FAS= facies successions, PSQ= parasequence, PSQS= parasequence set, Prog. = progradation, Aggr. = aggradation. M = mudstone, W = wackestone, P = packstone, G = grainstone, R = rudstone, B = boundstone.

Figure 16 Stratigraphic correlation of the studied sections based on the stratigraphic key surfaces (TS and MFS) and the lithofacies associations. See also Fig. 1 for location of sections T to MAD8019 (Zanzo). Sections U to Y are not represented here.

TS = transgressive surface represented by a heavy red line, MFS = maximum flooding surface represented by a heavy dark line. Filled and unfilled arrows represent respectively complete and uncomplete aggradational phases in TST (transgressive system tract) sedimentation. TS = transgressive surface, MFS = maximum flooding surface. See text and Fig. 17 for details. Dark arrows= aggradation (sections K, H, D, B and Zanzo).

Figure 17 Tentative sequence stratigraphic correlation of the SCI Subgroup between the Niari-Nyanga and Comba subbasins (RC) and Lower Congo subbasin (RDC) with two transgressive-regressive third-order sequences. The TST sedimentation is recorded in the SCIa and the lower SCIb in RC, and in the C1 Formation and C2a and C2b members in DRC. The SCIb in RC, and its stratigraphic coeval C2c to C2e members in DRC is marked by a HST phase. The SCIb-SCIc transition is characterized by a LST sedimentation of shallow water deposits (FA3/FA4, with abundant S2 cycles), which is also recorded in the C2f to C2h members in DRC. The LST phase is topped by a transgressive surface (TS) leading to TST sedimentation ('deep' MISS facies) until the maximum flooding surface (MFS) initiating the HST sedimentation with giant stromatolites, which are coeval with the C3a Member in DRC. The top of the SCI_c, and its stratigraphic equivalent C3b Member in DRC, is marked by

deposition of silty evaporites (LST) at the transition SCI-SCII. TS, MFS and SB (sequence boundaries) are indicated respectively by heavy dark and red lines. LST = lowstand system tract, TST = transgressive system tract, HST = highstand system tract, FRST= Forced regression system tract.

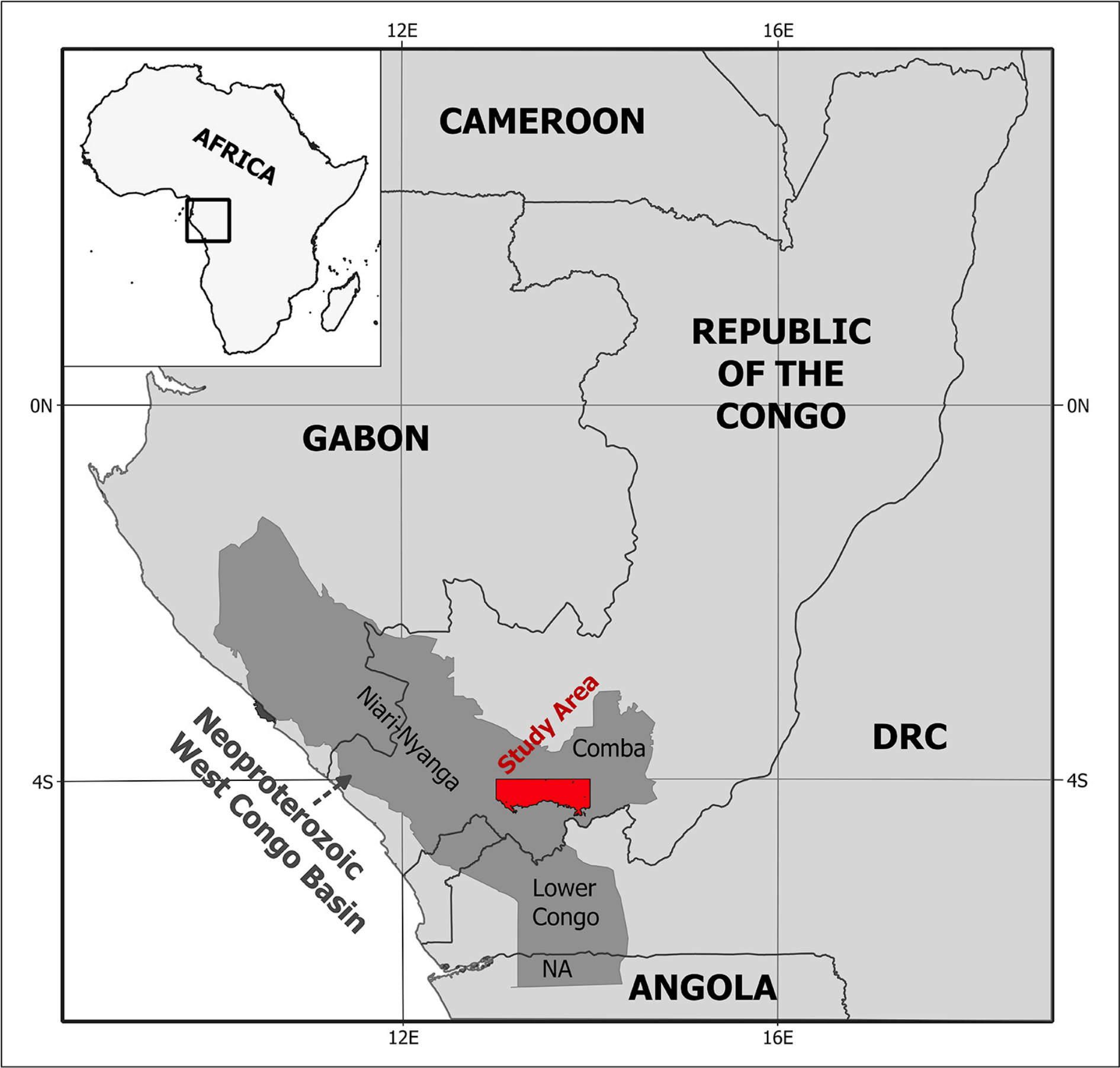
12E
16E
AFRICA
CAMEROON
REPUBLIC
OF THE
CONGO
0N
GABON
Niari-Nyanga
Study Area
Comba
DRC
4S
Neoproterozoic
West Congo Basin
Lower
Congo
NA
ANGOLA
12E
16E

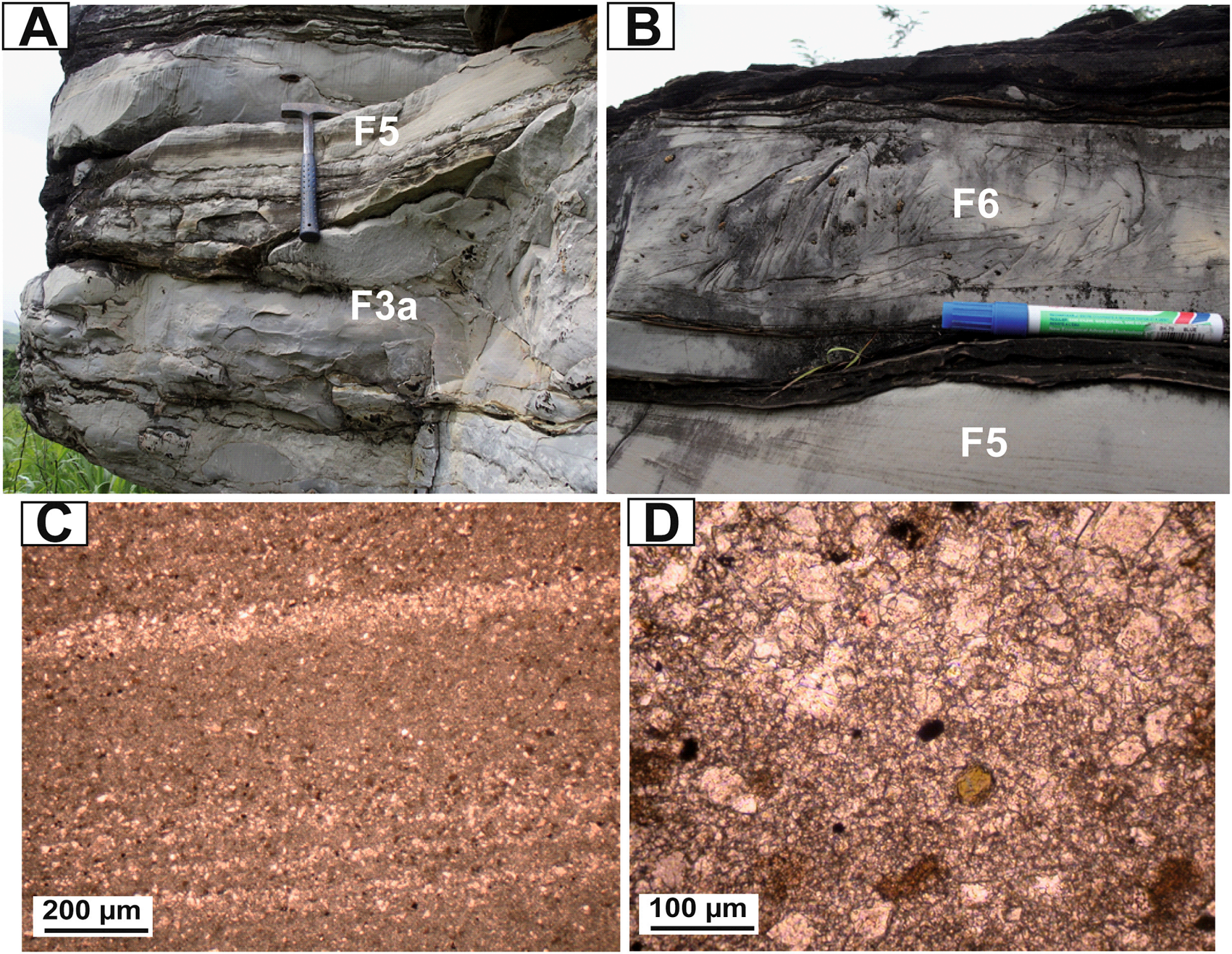
A
F5
F3a
B
F6
F5
C
200 µm
D
100 µm

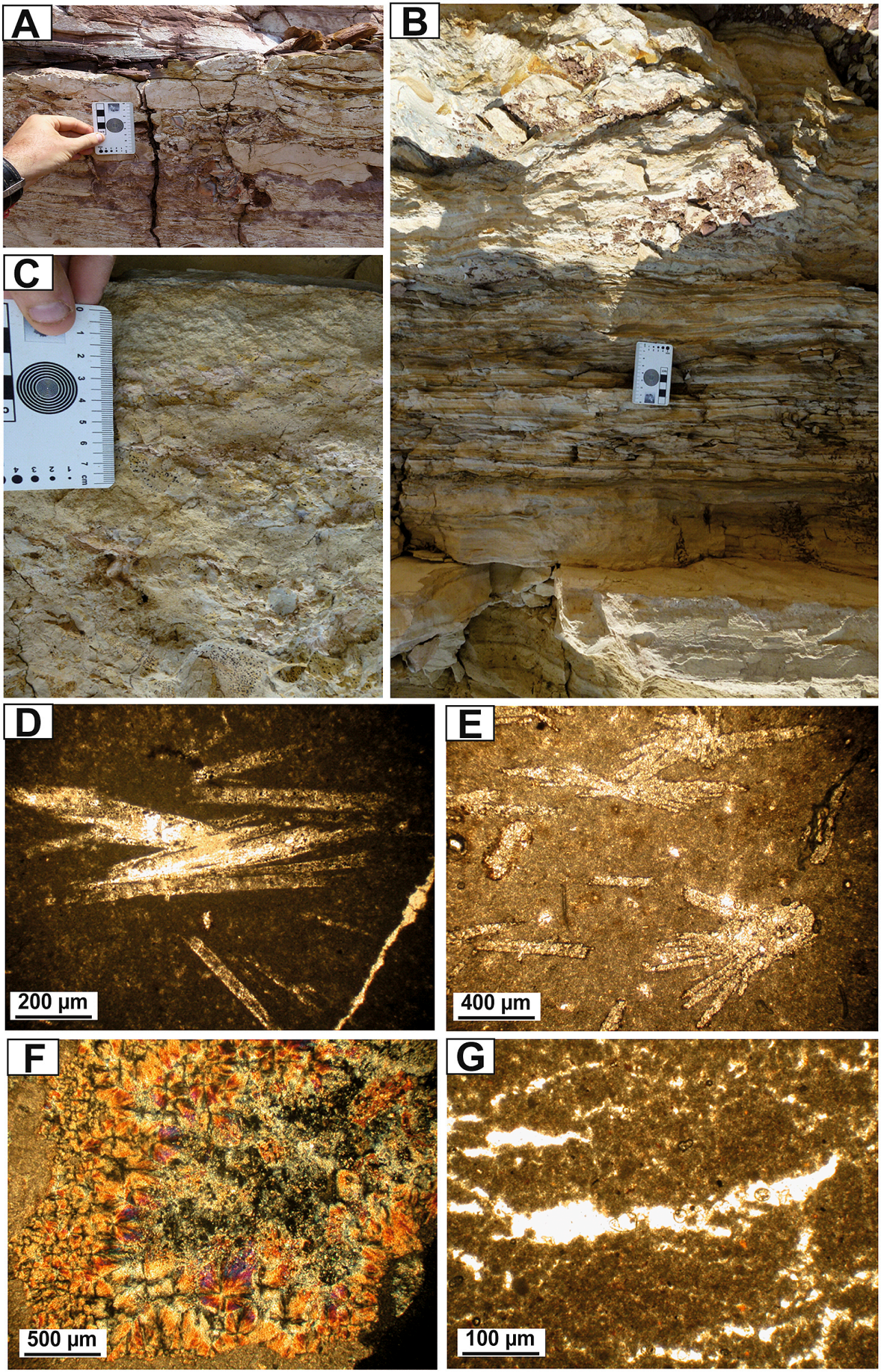
A
B
C
D
200 µm
E
400 µm
F
500 µm
G
100 µm

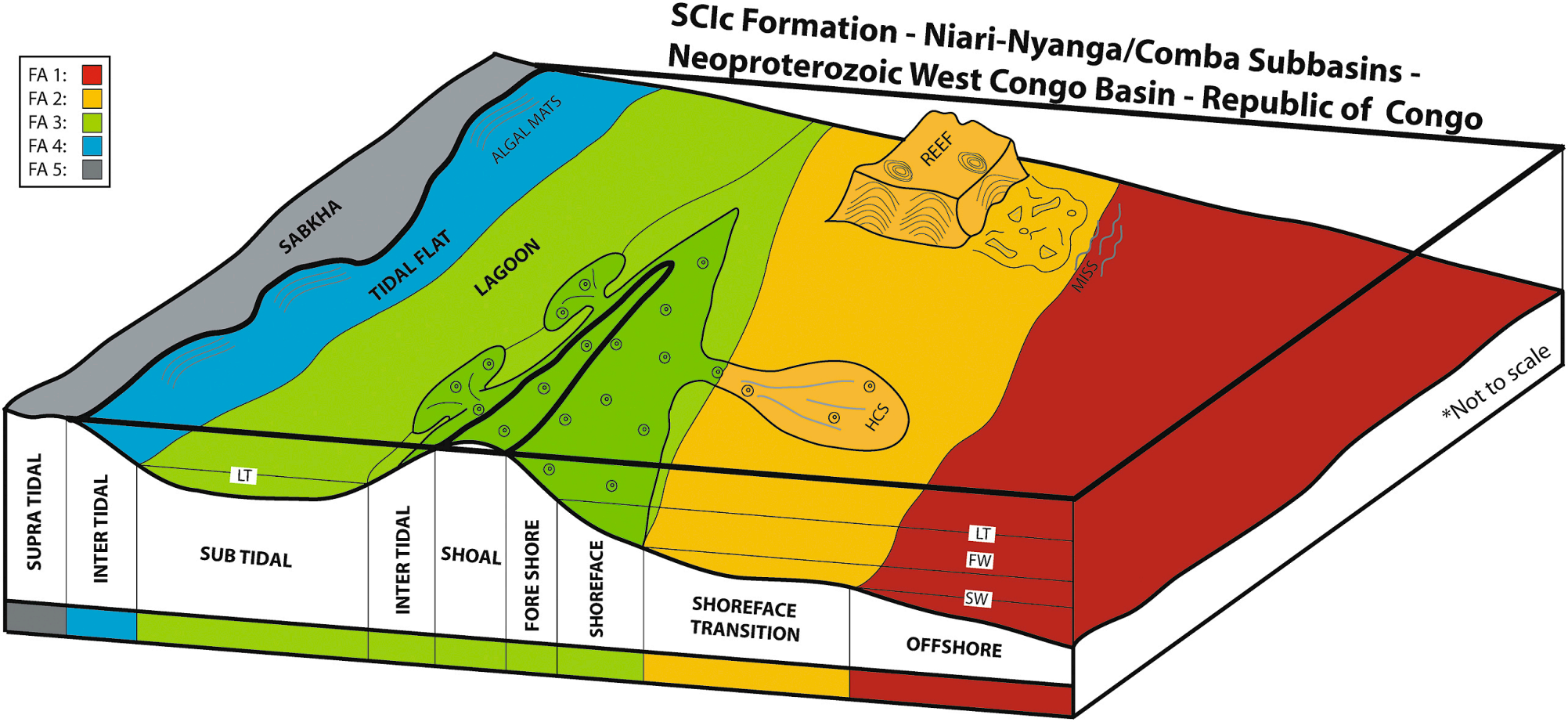
SCIc Formation - Niari-Nyanga/Comba Subbasins -
Neoproterozoic West Congo Basin - Republic of Congo
FA 1:
FA 2:
FA 3:
FA 4:
FA 5:
SABKHA
ALGAL MATS
TIDAL FLAT
LAGOON
REEF
MISS
HCS
LT
LT
FW
SW
SUPRA TIDAL
INTER TIDAL
SUB TIDAL
INTER TIDAL
SHOAL
FORE SHORE
SHOREFACE
SHOREFACE TRANSITION
OFFSHORE
*Not to scale

Peritidal cycles

Cycle S1

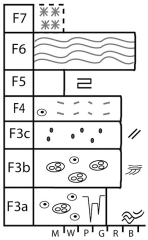

Cycle S2

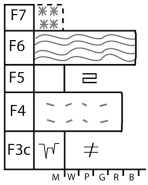

Cycle S3

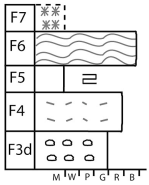

Deep cycles

Cycle D1

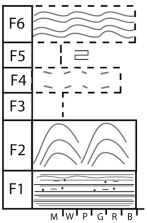

Cycle D2

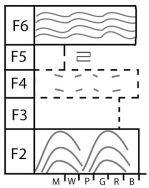

Legend

- Oolite
- Pisoid
- Peloid / micritic ooid
- Aggregate
- Domal Stromatolite
- Intraformational conglomerate
- Planar stromatolite
- Evaporite

Cycle S1

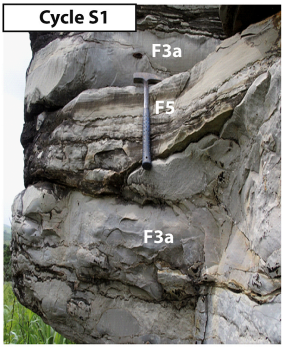

Cycle S2

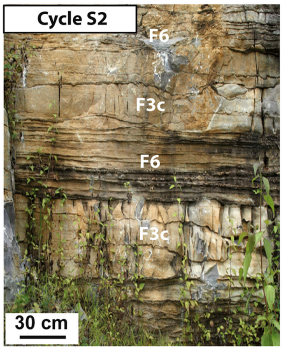

Cycle S3

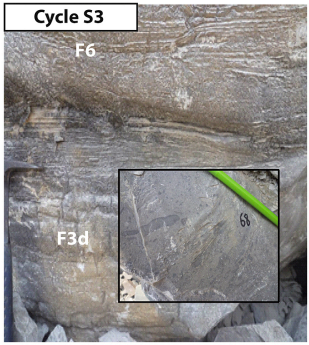

Cycle D1

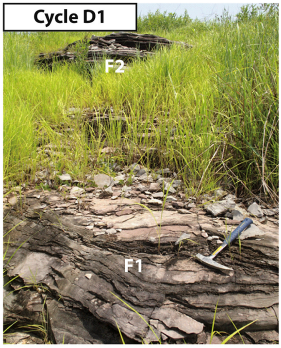

Cycle D2

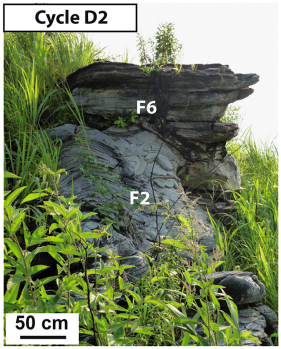

Legend

- Hummocky cross stratification
- Cross stratification
- Planar stratification
- No stratified (homogeneous)
- Angular stratification
- Stylolite

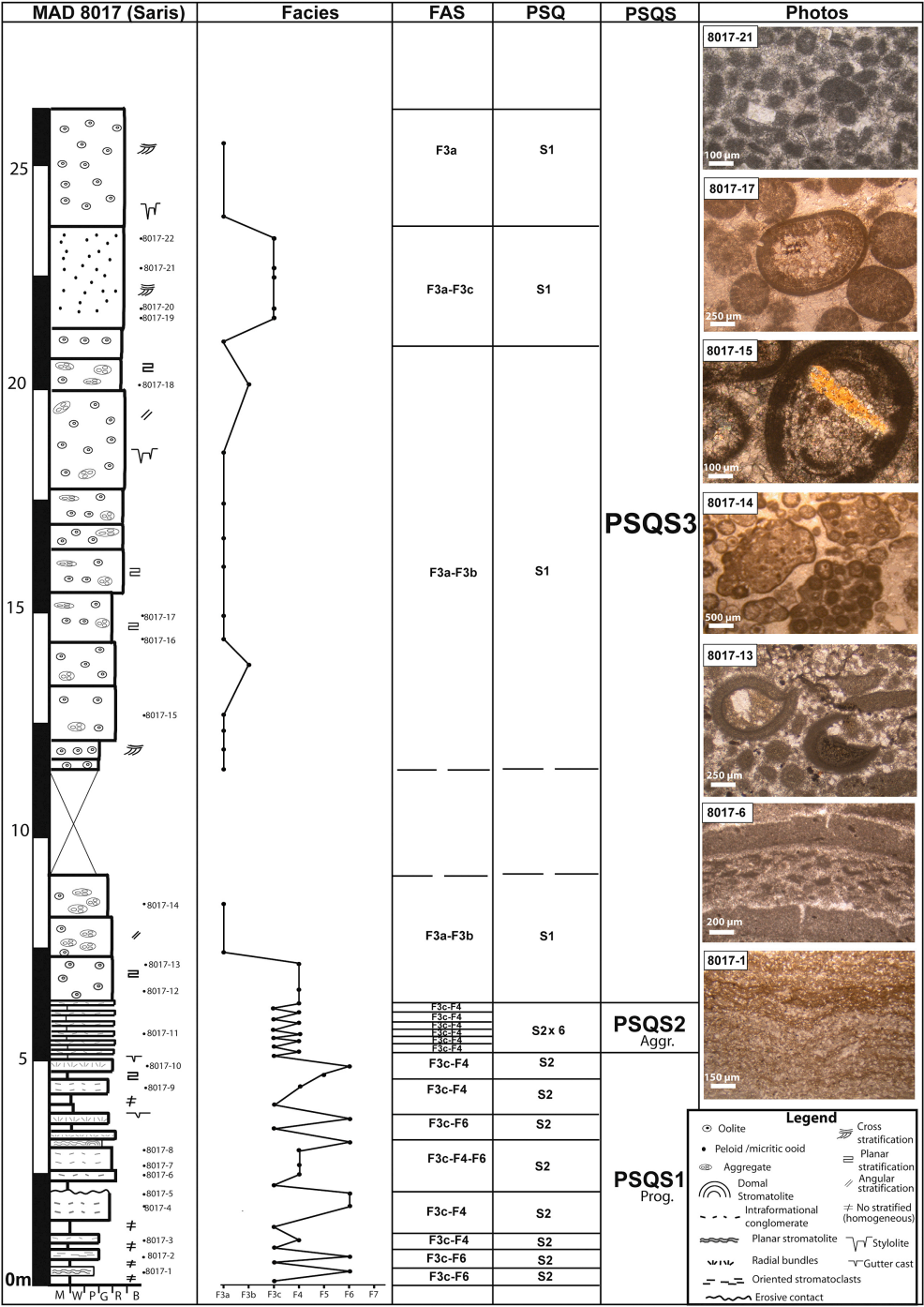
MAD 8017 (Saris)
Facies
FAS
PSQ
PSQS
Photos
25
20
15
10
5
0m
•8017-22
•8017-21
•8017-20
•8017-19
•8017-18
•8017-17
•8017-16
•8017-15
•8017-14
•8017-13
•8017-12
•8017-11
•8017-10
•8017-9
•8017-8
•8017-7
•8017-6
•8017-5
•8017-4
•8017-3
•8017-2
•8017-1
M W P G R B
F3a
F3a-F3c
F3a-F3b
F3a-F3b
F3c-F4
F3c-F4
F3c-F4
F3c-F4
F3c-F4
F3c-F4
F3c-F4
F3c-F4
F3c-F6
F3c-F4-F6
F3c-F4
F3c-F4
F3c-F6
F3c-F6
S1
S1
S1
S2x 6
S2
S2
S2
S2
S2
S2
S2
S2
PSQS3
PSQS2
Aggr.
PSQS1
Prog.
F3a F3b F3c F4 F5 F6 F7
8017-21
100 µm
8017-17
250 µm
8017-15
100 µm
8017-14
500 µm
8017-13
250 µm
8017-6
200 µm
8017-1
150 µm
Legend
Oolite
Peloid /micritic ooid
Aggregate
Domal Stromatolite
Intraformational conglomerate
Planar stromatolite
Radial bundles
Oriented stromatoclasts
Erosive contact
Cross stratification
Planar stratification
Angular stratification
No stratified (homogeneous)
Stylolite
Gutter cast

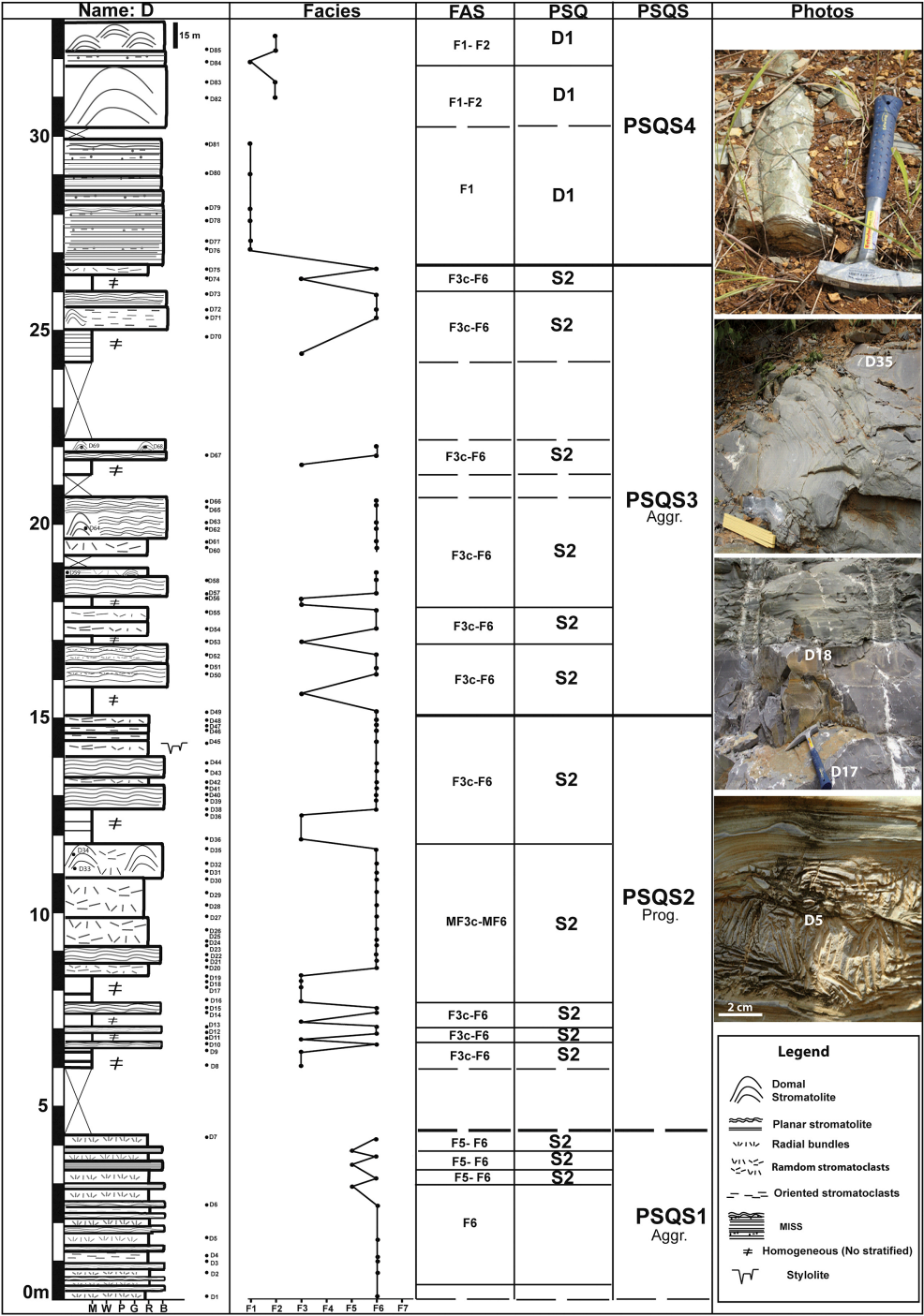
Name: D
Facies
FAS
PSQ
PSQS
Photos
15 m
30
25
20
15
10
5
0m
M W P G R B
F1 F2 F3 F4 F5 F6 F7
F1- F2
F1-F2
F1
F3c-F6
MF3c-MF6
F5- F6
F6
D1
S2
PSQS4
PSQS3
Aggr.
PSQS2
Prog.
PSQS1
Aggr.
D35
D18
D17
D5
2 cm
Legend
Domal Stromatolite
Planar stromatolite
Radial bundles
Ramdom stromatoclasts
Oriented stromatoclasts
MISS
Homogeneous (No stratified)
Stylolite

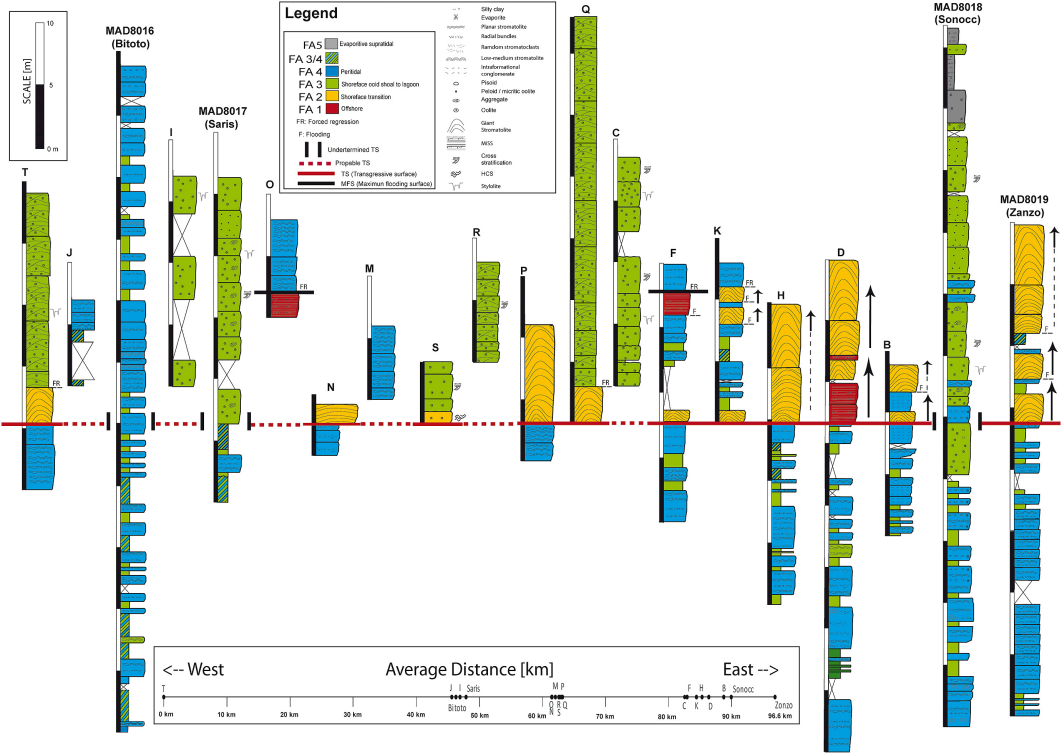
SCALE [m]
10
5
0 m
Legend
FA5 Evaporitive supratidal
FA 3/4
FA 4 Peritidal
FA 3 Shoreface cold shoal to lagoon
FA 2 Shoreface transition
FA 1 Offshore
FR: Forced regression
F: Flooding
Undetermined TS
Propable TS
TS (Transgressive surface)
MFS (Maximun flooding surface)
Silty clay
Evaporite
Planar stromatolite
Radial bundles
Random stromatolaits
Low-medium stromatolite
Intraformational conglomerate
Pisoid
Peloid / micritic oolite
Aggregate
Oolite
Giant Stromatolite
MISS
Cross stratification
HCS
Stylolite
MAD8016 (Bitoto)
MAD8017 (Saris)
MAD8018 (Sonocc)
MAD8019 (Zanzo)
T
J
I
O
N
M
S
R
P
Q
C
F
K
H
D
B
FR
F
<-- West
Average Distance [km]
East -->
T
J I Saris
M P
F H
B Sonocc
Bitoto
O R Q
N S
C K D
Zonzo
0 km
10 km
20 km
30 km
40 km
50 km
60 km
70 km
80 km
90 km
96.6 km

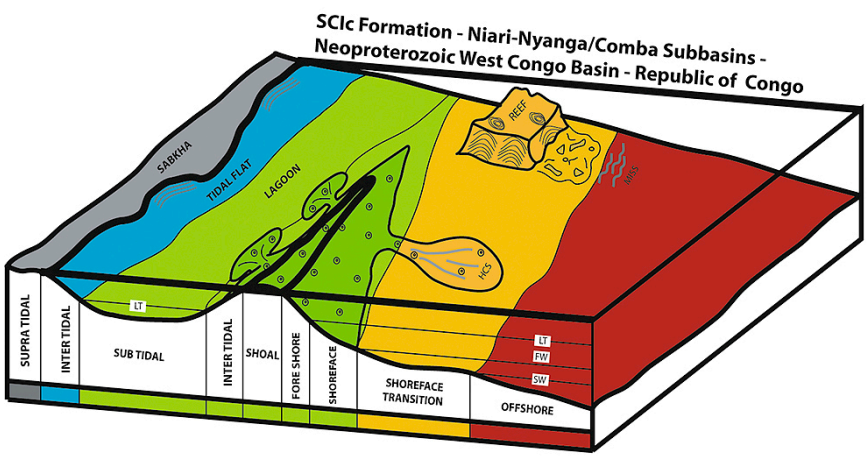
SCIc Formation - Niari-Nyanga/Comba Subbasins -
Neoproterozoic West Congo Basin - Republic of Congo
SABKHA
TIDAL FLAT
LAGOON
REEF
MISS
MCS
LT
SUPRA TIDAL
INTER TIDAL
SUB TIDAL
INTER TIDAL
SHOAL
FORE SHORE
SHOREFACE
SHOREFACE TRANSITION
OFFSHORE
LT
FW
SW

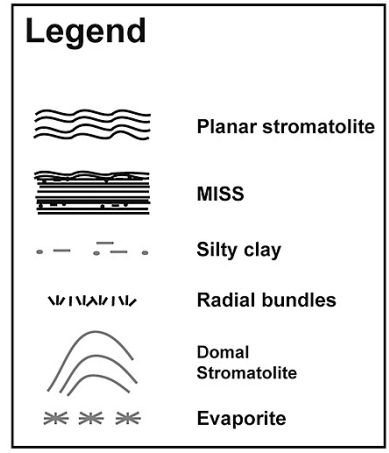
Legend
Planar stromatolite
MISS
Silty clay
Radial bundles
Domal Stromatolite
Evaporite

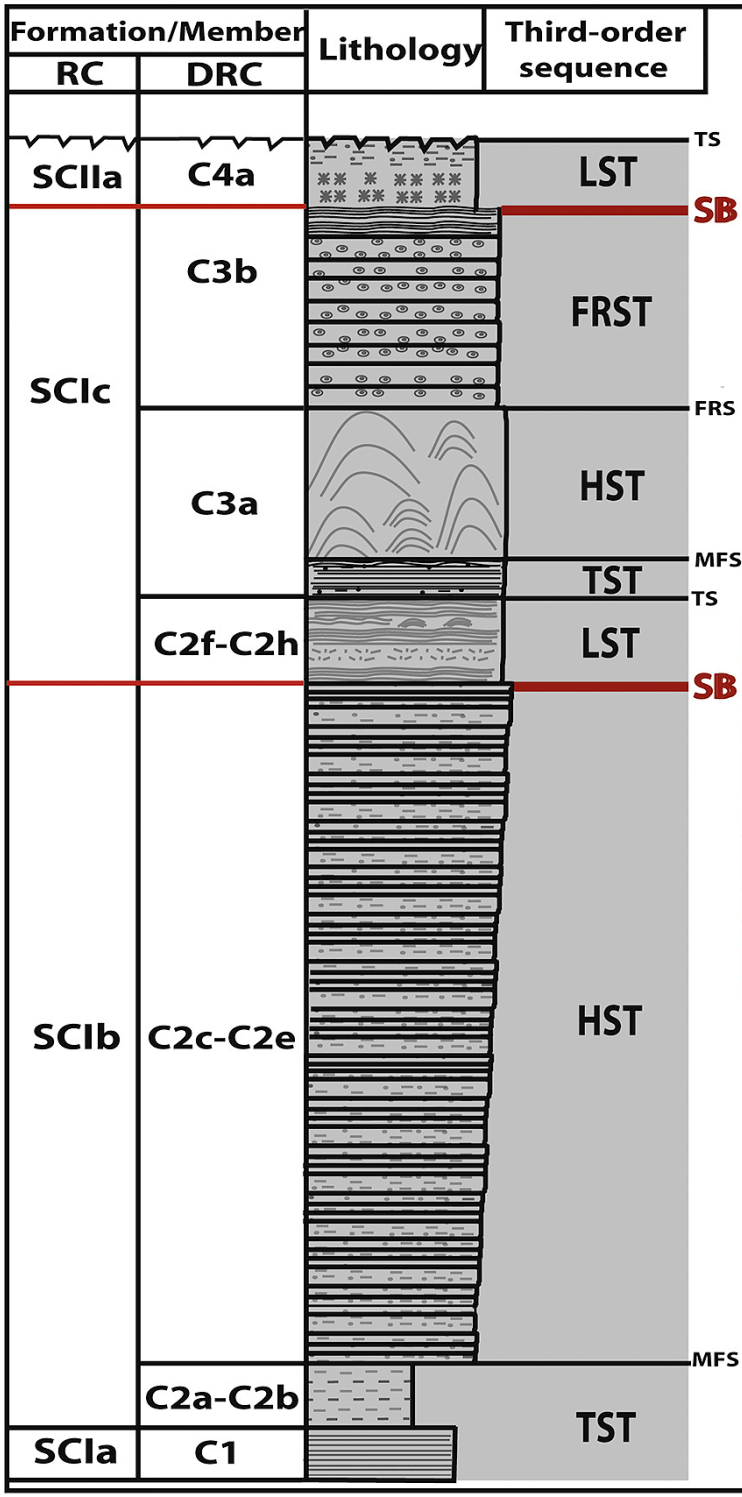
Formation/Member
RC
DRC
Lithology
Third-order sequence
SCIIa
C4a
LST
TS
SB
SCIc
C3b
FRST
FRS
C3a
HST
MFS
TST
TS
C2f-C2h
LST
SB
SCIb
C2c-C2e
HST
MFS
C2a-C2b
TST
SCIa
C1
25 m

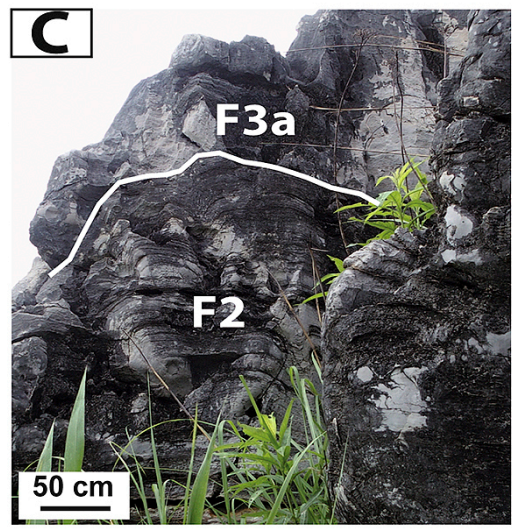
C
F3a
F2
50 cm


B

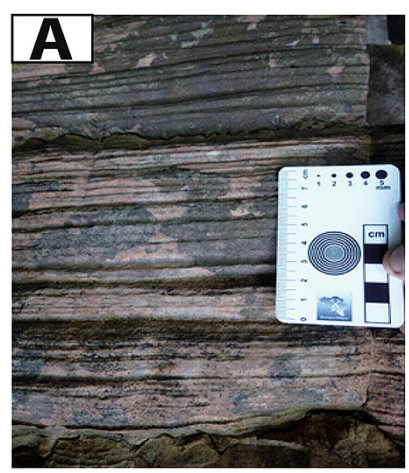
A

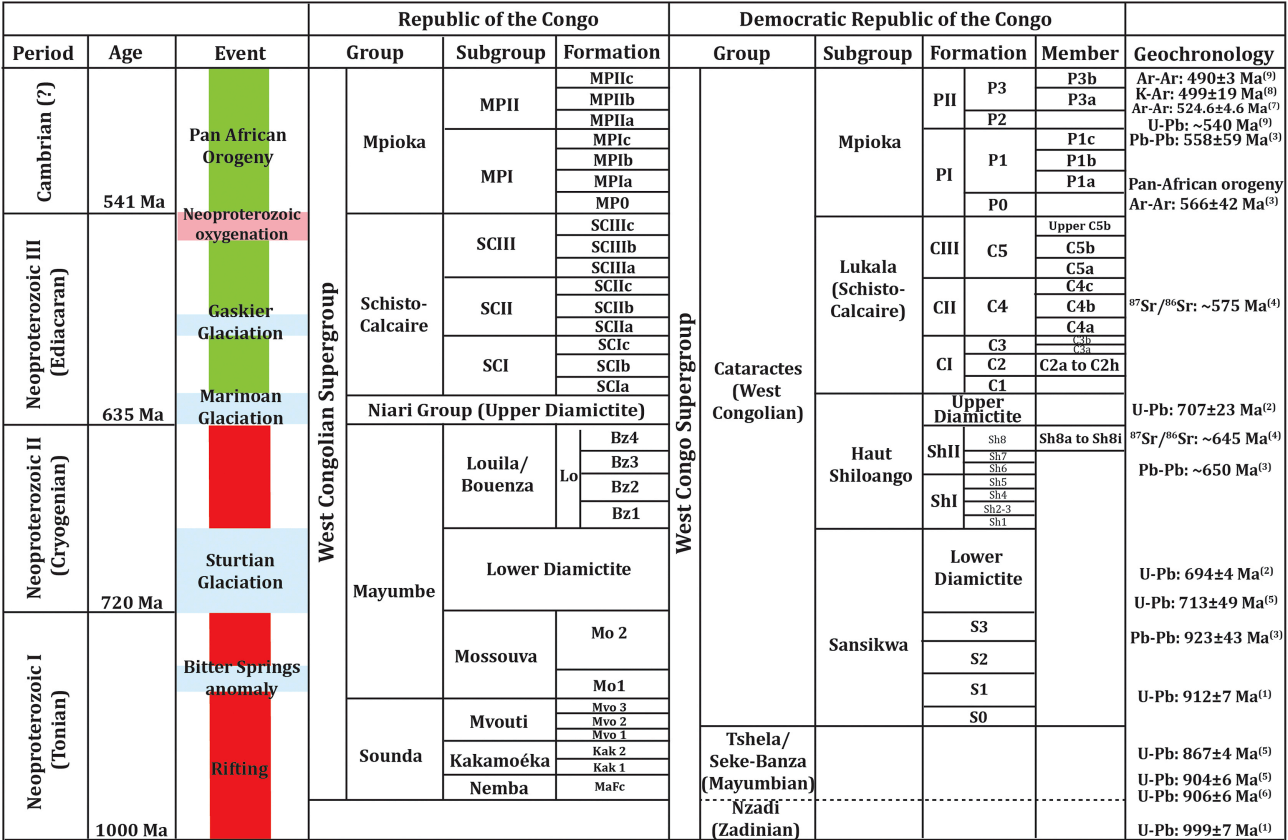

(1) Tack et al. (2001), (2) Straathof (2011), (3) Frimmel et al. (2006), (4) Poidevin (2007), (5) Thiéblemont et al. (2009), (6) Charles et al. (2015), (7) Tack et al. (2018), (8) Fullgraff et al. (2015), (9) Monié et al. (2012)

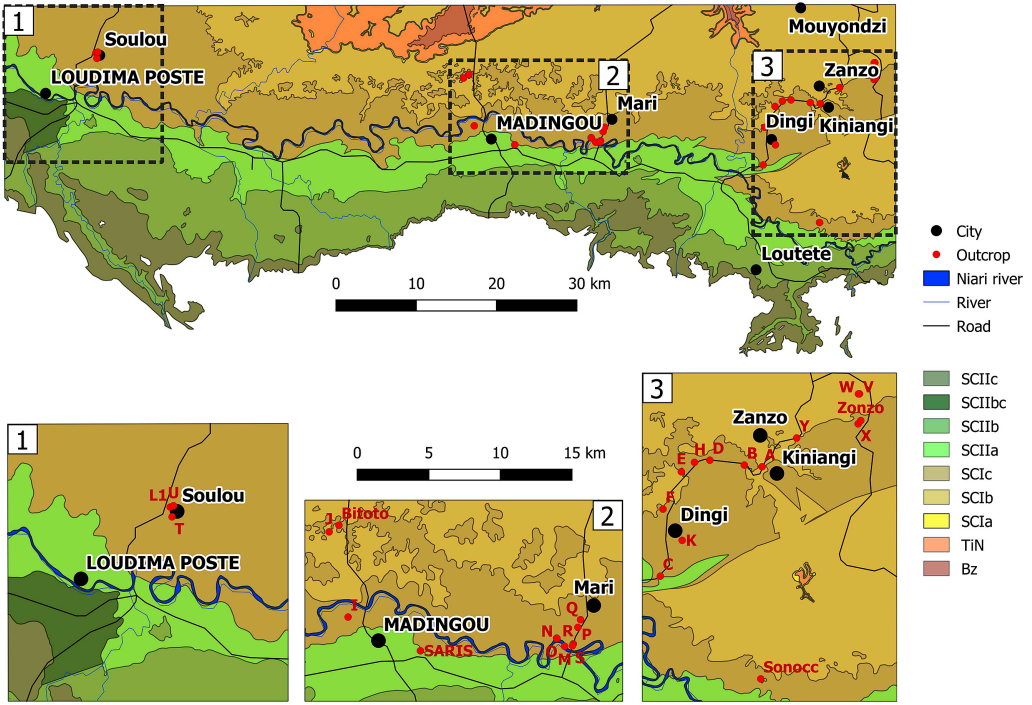
1
Soulou
LOUDIMA POSTE
2
Mari
MADINGOU
3
Mouyondzi
Zanzo
Dingi
Kiniangi
Loutete
0 10 20 30 km
City
Outcrop
Niari river
River
Road
SCIIc
SCIIbc
SCIIb
SCIIa
SCIc
SCIb
SCIa
TiN
Bz
1
L1U
Soulou
T
LOUDIMA POSTE
0 5 10 15 km
2
1
Bifoto
Mari
MADINGOU
SARIS
Q
N
R
P
O
M
3
W
V
Zonzo
Zanzo
Y
X
Kiniangi
H
D
E
B
A
F
Dingi
K
C
Sonocc

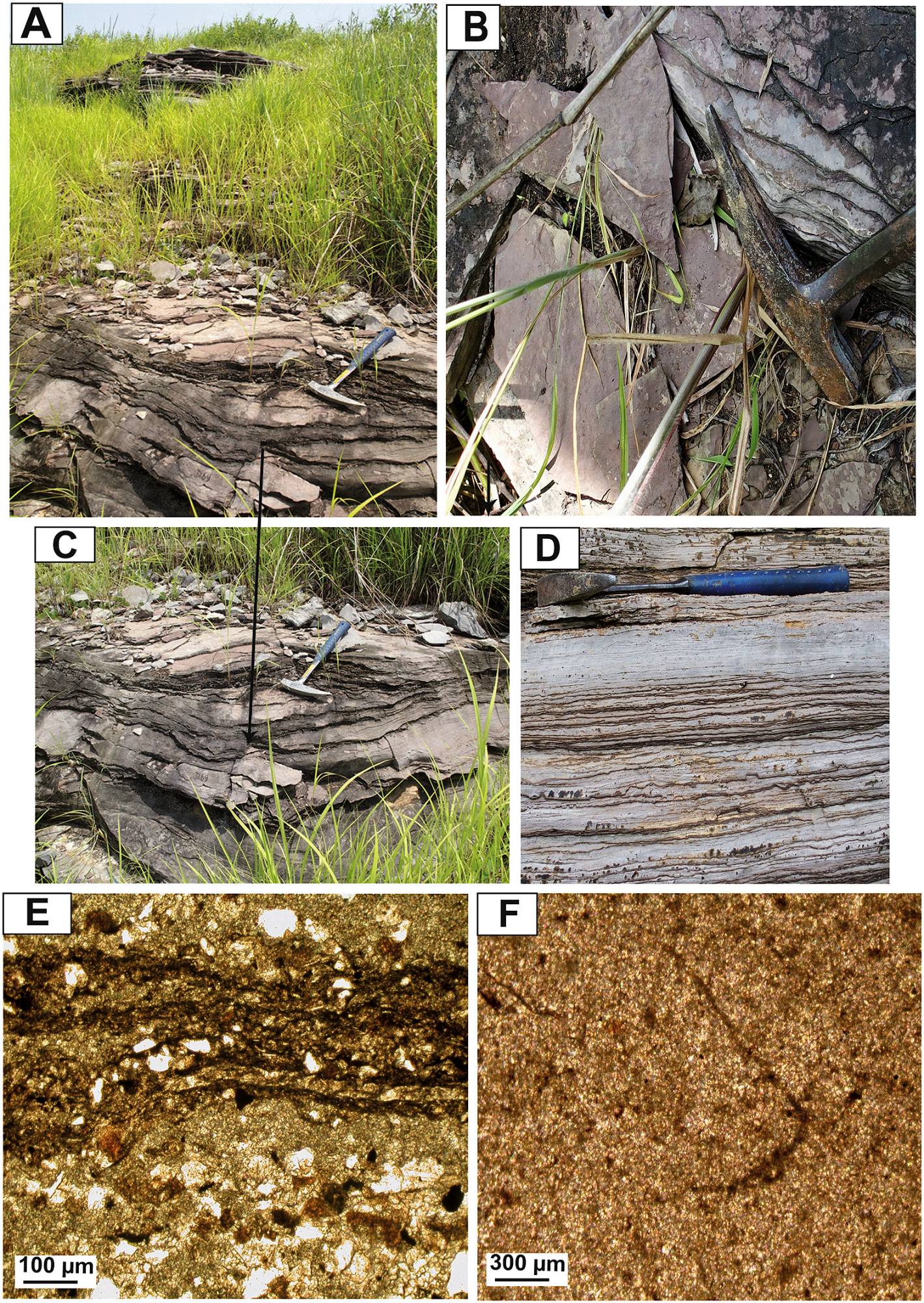
A
B
C
D
E
100 µm
F
300 µm


A


B


C

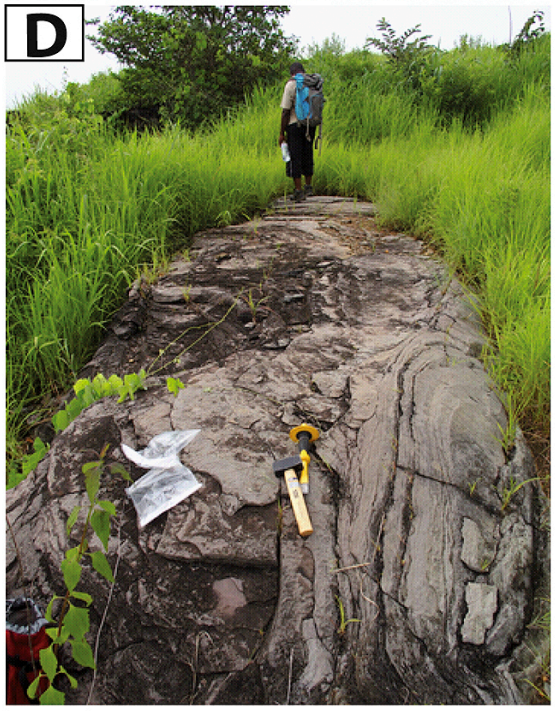
D


E


G


F

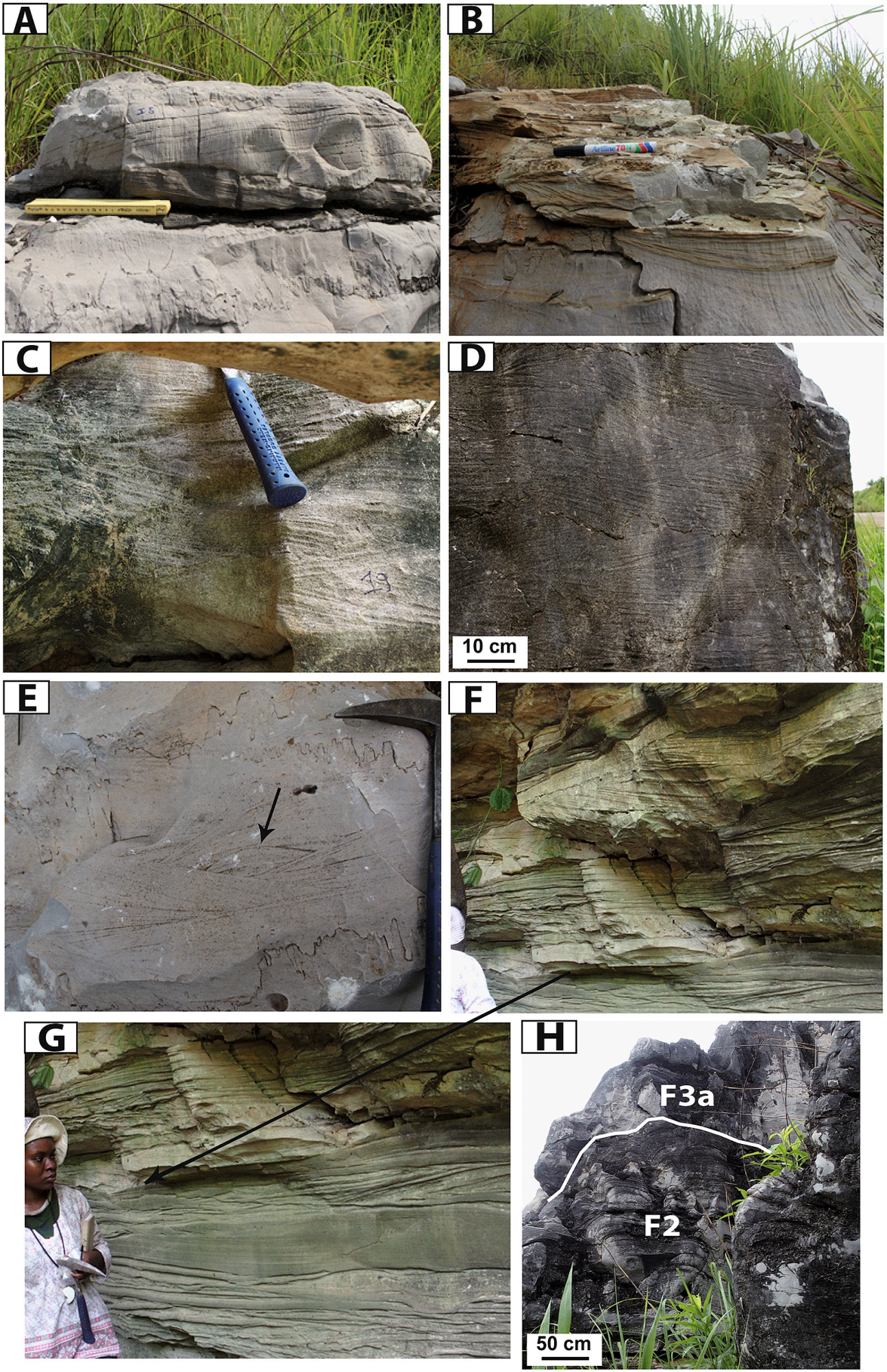
A
B
C
D
10 cm
E
F
G
H
F3a
F2
50 cm

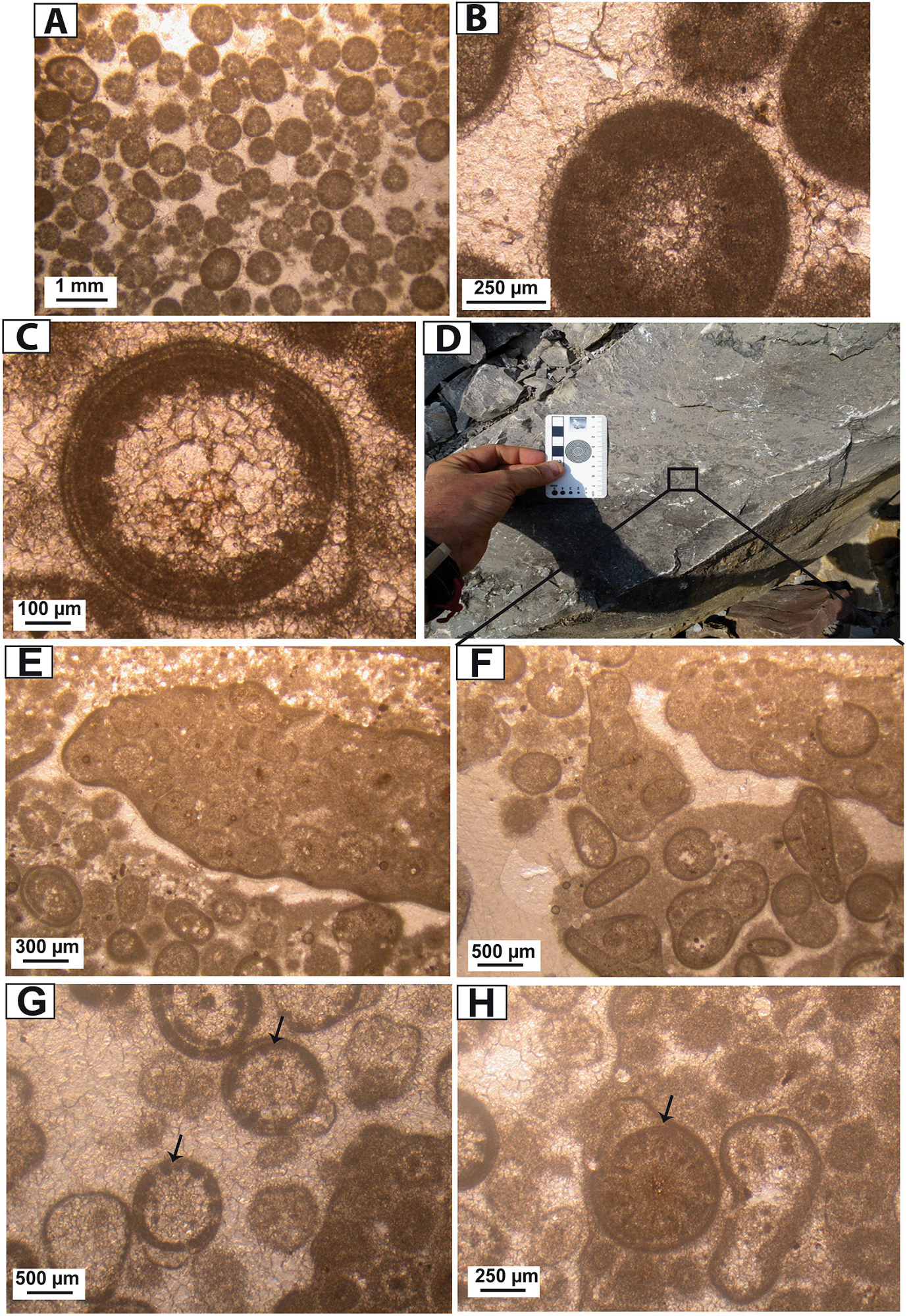
A
1 mm
B
250 µm
C
100 µm
D
E
300 µm
F
500 µm
G
500 µm
H
250 µm

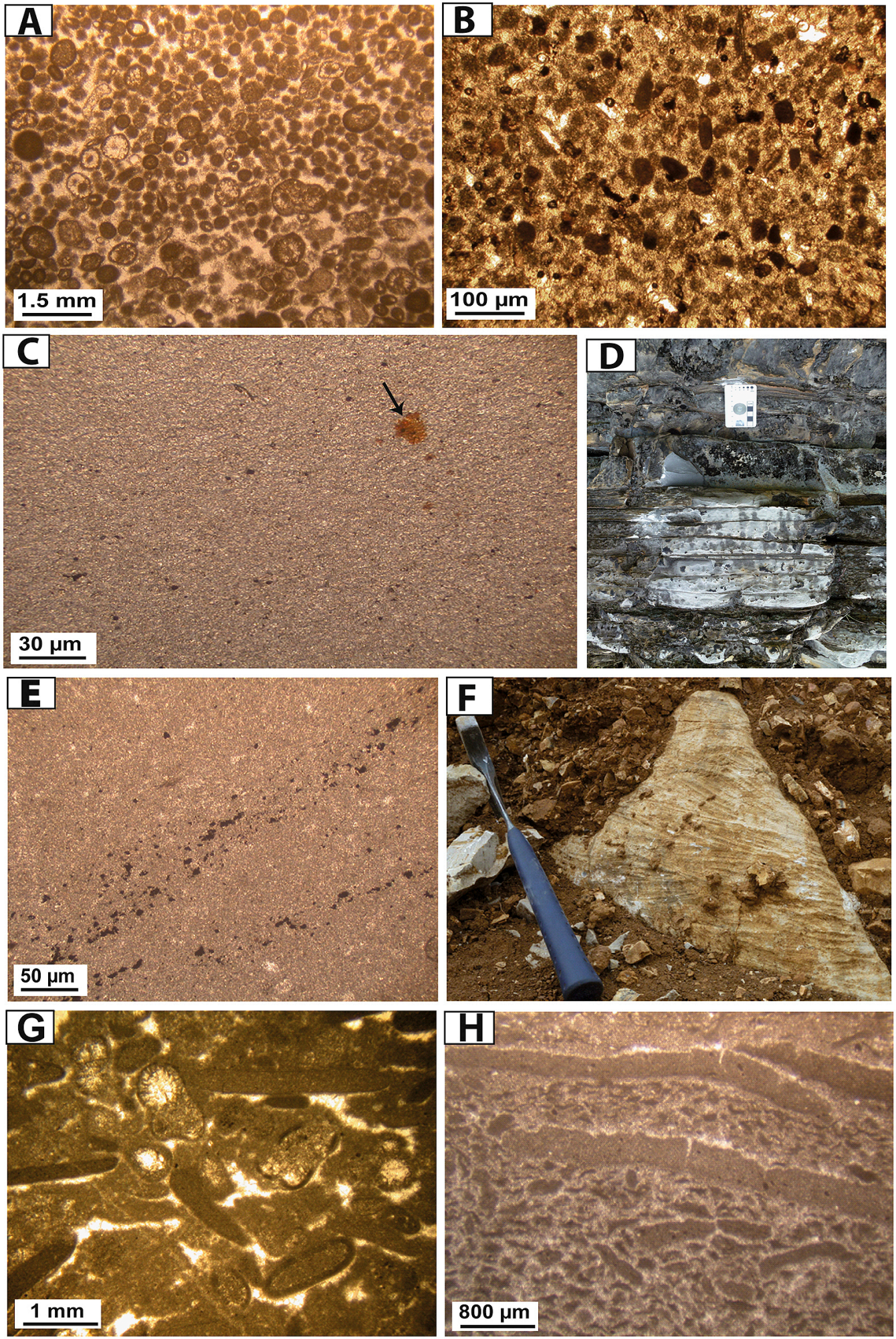
A
1.5 mm
B
100 µm
C
30 µm
D
E
50 µm
F
G
1 mm
H
800 µm

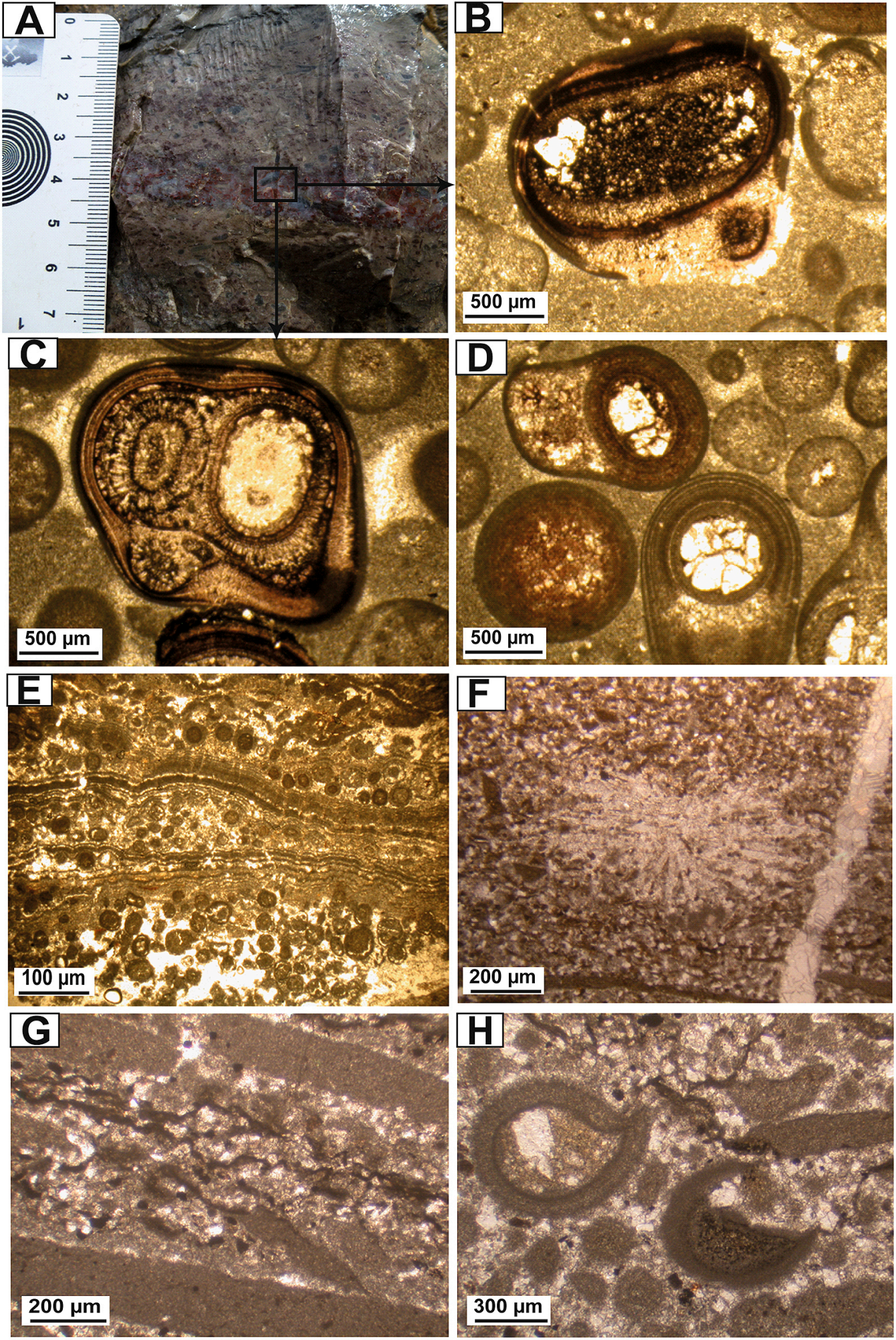
A
B
500 µm
C
500 µm
D
500 µm
E
100 µm
F
200 µm
G
200 µm
H
300 µm

LOG (EPSG:4326 WGS 84)	Latitude	Longitude	Elevation
A	S04°06.687'	E013°54.922'	265m
B	S04°06.621'	E013°54.251'	341m
C	S04°10.824'	E013°51.076'	215m
D	S04°06.436'	E013°52.951'	321m
E	S04°06.874'	E013°51.875'	241m
F	S04°08.285'	E013°51.181'	242m
G	S04°14.720'	E013°54861'	230m
H	S04°06.517'	E013°52.372'	297m
I	S04°08.150'	E013°31.619'	196m
J	S04°04.922'	E013°30.908'	262m
K	S04°09.470'	E013°51.901'	215 m
L1	S04°03.170'	E013°06.155'	202m
M	S04°09.271'	E013°39.792’	138m
N	S04°08.965'	E013°39.493’	140m
O	S04°08.973'	E013°39.504'	140m
P	S04°08.557’	E013°40.295’	190m
Q	S04°08.266’	E013°40.397’	201m
R	S04°09.180’	E013°40.121’	153m
S	S04°09.252’	E013°40.090’	144m
T	S04°03.540'	E013°06.225'	198m
U	S04°03.119'	E013°06.282'	236m
V	S04°03.931'	E013°58.601’	446m
W	S04°03.933’	E013°58.561’	446m
X	S04°05.066'	E013°58.548'	395m
Y	S04°05.600'	E013°56.229'	371m
MAD8016 (Bitoto)	S04°04.672'	E013°31.278'	268m
MAD8019 (Zanzo)	S04°04.944'	E013°58.648'	370m
MAD8018 (Sonocc)	S04°14.720'	E013°54.861'	230m
MAD8017 (Saris)	S04°09.433'	E013°34.348'	164m

Journal Pre-proof

Type	Cycle features
S3	This cycle is relatively rare and less than 1.5 m-thick. The succession consists of pisoidic grainstone/floatstone, intraformational conglomerate, laminar detrital mudstone overlain by laminar microbial mats and evaporitive mudstone with abundant pseudomorphs after sulphates. Meniscus and pendular cements, keystone vugs, desiccation cracks are present. Beds are sometimes lenticular.
S2	This cycle is the most common, with thickness from a few cm to 7 m. It is a homogeneous mudstone overlain by an intraformational conglomerate, laminar detrital mudstone and topped by stratiform stromatolites, brecciated or not. Desiccation cracks, vadose cements, pseudomorphs of evaporative crystals are common. Beds are lenticular or not.
S1	Thickness varies from 0.8 m to 5 m with variable internal composition. The cycle is a succession of ooid grainstone/packstone, floatstone/packstone with abundant aggregates, peloidal grainstone/packstone, intraformational conglomerate, laminar detrital mudstone topped by stratiform stromatolites. Vadose cementation occurs. Beds must be lenticular.
D2	The cycle varies from 2 m to 10 m. The base of the cycle is a biohermal stromatolite (> 1 m) overlain by ooid grainstone/packstone or homogeneous mudstone, intraformational conglomerate, laminar detrital and by stratiform stromatolites in the top. Stromatolites show no evidence of exposure.
D1	The thickness ranges from 4 m to 20 m. The cycle is characterized by purplish laminar clayey and silty mudstones topped by giant stromatolites with no evidence of subaerial exposure.

Type	Cycle features
S3	This cycle is relatively rare and less than 1.5 m-thick. The succession consists of pisoidic grainstone/floatstone, intraformational conglomerate, laminar detrital mudstone overlain by laminar microbial mats and evaporitive mudstone with abundant pseudomorphs after sulphates. Meniscus and pendular cements, keystone vugs, desiccation cracks are present. Beds are sometimes lenticular.
S2	This cycle is the most common, with thickness from a few cm to 7 m. It is a homogeneous mudstone overlain by an intraformational conglomerate, laminar detrital mudstone and topped by stratiform stromatolites, brecciated or not. Desiccation cracks, vadose cements, pseudomorphs of evaporative crystals are common. Beds are lenticular or not.
S1	Thickness varies from 0.8 m to 5 m with variable internal composition. The cycle is a succession of ooid grainstone/packstone, floatstone/packstone with abundant aggregates, peloidal grainstone/packstone, intraformational conglomerate, laminar detrital mudstone topped by stratiform stromatolites. Vadose cementation occurs. Beds must be lenticular.
D2	The cycle varies from 2 m to 10 m. The base of the cycle is a biohermal stromatolite (> 1 m) overlain by ooid grainstone/packstone or homogeneous mudstone, intraformational conglomerate, laminar detrital and by stratiform stromatolites in the top. Stromatolites show no evidence of exposure.
D1	The thickness ranges from 4 m to 20 m. The cycle is characterized by purplish laminar clayey and silty mudstones topped by giant stromatolites with no evidence of subaerial exposure.

Saris section

The Saris section (Fig. 14) shows well-developed S2 cycles in the lower part with dominant S1 cycles in the upper part. It consists of 11 meter- to plurimeter-scale cycles with a pronounced thickening-upward trend at the fourth-order. The mean thickness is 0.85 m for the S2 cycles (ranging from 0.4-1.3 m) and is 6.5 m (ranging from 3.0-11.5 m) for the S1 cycles.

Two parasequences sets are present, the first one with S2 cycles is aggradational and the second one with S1 cycles is strongly progradational.

D section

The D section (Fig. 15) shows dominated S2 parasequences overlain by open marine D1 parasequences. It is composed of centimeter- to meter-scale facies assemblages with 73 elementary S2 parasequences and, in its upper part two plurimetric D1.

Four parasequence sets are recognized (i) aggradational 1 (minimum 4.2 m-thick) with very thin S2 cycles without thickness evolution, (ii) progradational 2 (at least 10.8 m-thick with 5 metric S2 cycles, averaging 2.2 m and ranging from 0.6-4 m), (iii) aggradational 3 with at least six S2 cycles (9.9 m-thick, averaging 1.7 m) without clear thickness evolution, (iii) aggradational 3 (at least 6.3 m-thick) and (iv) progradational 4 (± 25 m-thick) with at least two D1 cycles showing a pronounced thickening-upward evolution.

Highlights

1. The SCIc Formation records the evolution of a marine ramp
2. It is a carbonate succession of meter-scale shallowing-upward cycles
3. The cycles are the result of the interplay of relative sea-level changes
4. The SCI_c cycles are enclosed into a third-order sequence related to the deposition of the SCI Subgroup

Declaration of interests

☒ The authors declare that they have no known competing financial interests or personal relationships that could have appeared to influence the work reported in this paper.

☐The authors declare the following financial interests/personal relationships which may be considered as potential competing interests: